Study of $B_s \to K^{(*)}\ell^+\ell^-$ decays in the PQCD factorization approach with lattice QCD input

Su-Ping Jin,[1,*] Xue-Qing Hu,[1,†] and Zhen-Jun Xiao[1,2,‡]

[1]*Department of Physics and Institute of Theoretical Physics, Nanjing Normal University, Nanjing, Jiangsu 210023, People's Republic of China*

[2]*Jiangsu Key Laboratory for Numerical Simulation of Large Scale Complex Systems, Nanjing Normal University, Nanjing 210023, People's Republic of China*

(Received 31 March 2020; accepted 22 June 2020; published 7 July 2020)

In this paper, we studied systematically the semileptonic decays $\bar{B}_s \to K^{(*)}\ell^+\ell^-$ with $l^- = (e^-, \mu^-, \tau^-)$ by using the perturbative QCD (PQCD) and the "PQCD + Lattice" factorization approach, respectively. We first evaluated all relevant form factors $F_i(q^2)$ in the low-q^2 region using the PQCD approach, and we also took the available lattice QCD results at the end point $q^2_{\rm max}$ as additional inputs to improve the extrapolation of the form factors to the high-q^2 region. We calculated the branching ratios and twelve other kinds of physical observables. From our studies, we find the following points: (a) for $\bar{B}_s \to K l^+ l^-$ decays, the PQCD and PQCD + Lattice predictions for branching ratios $\mathcal{B}(\bar{B}_s \to K l^+ l^-)$, the ratios of the branching ratios $R_K^{e\mu}$ and $R_K^{\mu\tau}$, and the longitudinal polarization asymmetry of the leptons P_L agree well within errors; (b) the PQCD and PQCD + Lattice predictions for the CP-averaged branching ratio $\mathcal{B}(\bar{B}_s \to K^*\mu^+\mu^-)$ are $(3.17^{+0.95}_{-0.78}) \times 10^{-8}$ and $(2.48^{+0.56}_{-0.50}) \times 10^{-8}$ respectively, which agree well with the LHCb measured value $(2.9 \pm 1.1) \times 10^{-8}$ and the light-cone sum rule prediction; (c) for the ratios $R_{K^*}^{e\mu}$ and $R_{K^*}^{\mu\tau}$, the PQCD and PQCD + Lattice predictions agree well with each other and have a small error less than 10%; (d) for the direct CP asymmetries $\mathcal{A}_{CP}$ of all considered decay modes, they are always very small as expected: less than 5% in magnitude; (e) for the angular observables $P_{1,2,3}$ and $P'_{4,5,6,8}$, our theoretical predictions for each kind of lepton are consistent within errors; (f) the theoretical predictions of the angular observables P_3 and P'_6 are less than 10^{-2} in size, but the magnitude of $P_{1,2}$ and $P'_{4,5}$ are larger than 0.2; and (g) the PQCD and PQCD + Lattice predictions of the binned values of all considered observables in the two q^2 bins [0.1–0.98] GeV^2 and [1.1–6] GeV^2 generally agree with each other and are also consistent with the light-cone sum rule results within errors. We believe that above predictions could be tested by future LHCb and Belle-II experiments.

DOI: 10.1103/PhysRevD.102.013001

I. INTRODUCTION

The lepton flavor universality (LFU), as one of the distinctive hypotheses of the standard model (SM), requires the same kinds of couplings between the gauge bosons and the three families of leptons except for mass effects. However, the recently reported R_K and R_{K^*} anomalies bring a primary hint of the LFU violation. The measured values of the ratios R_K and R_{K^*}, defined as the ratios of the branching fractions (BRs) $\mathcal{B}(B \to K^{(*)}\mu^+\mu^-)$ and $\mathcal{B}(B \to K^{(*)}e^+e^-)$ [1], are clearly smaller than the SM predictions [2–8]: the deviation is about 2.6σ for R_K and 2.3σ for R_{K^*} [9–14]. In addition, the LHCb experiment first observed the so-called P'_5 anomaly, a sizeable discrepancy at 3.7σ between the measurement and the SM prediction in one bin for the angular observables P'_5 [15,16].

If the above mentioned anomalies are indeed the signal of the LFU violation in $b \to s\ell^+\ell^-$ decays, it must appear in the similar process $b \to d\ell^+\ell^-$, because they are the same kinds of flavor-changing neutral current (FCNC) transitions at the quark level with the differences of Cabibbo-Kobayashi-Maskawa (CKM) matrix elements (V_{td} vs V_{ts}) and the masses (m_d vs m_s). As a consequence of the Glashow-Iliopoulos-Maiani mechanism [17], the flavor structure of the SM theory permits the FCNC to arise at the loop level only, leaving some space for heavy new degrees of freedom to contribute to these rare

*2223919088@qq.com
†hu-xueqing@qq.com
‡xiaozhenjun@njnu.edu.cn

processes [18]. With the same quark level $b \to d\mu^+\mu^-$ transitions, the exclusive $B^\pm \to \pi^\pm\mu^+\mu^-$ and $B_s^0 \to \bar{K}^{*0}\mu^+\mu^-$ decays have been measured recently by the LHCb experiment [19,20]:

$$\mathcal{B}(B^\pm \to \pi^\pm\mu^+\mu^-) = (1.83 \pm 0.24(\text{stat.}) \pm 0.05(\text{syst.})) \times 10^{-8}, \quad (1)$$

$$\mathcal{B}(B_s^0 \to \bar{K}^{*0}\mu^+\mu^-) = (2.9 \pm 1.0(\text{stat.}) \pm 0.2(\text{syst.}) \pm 0.3(\text{norm.})) \times 10^{-8}, \quad (2)$$

and they agree well with those currently available SM predictions as given, for example, in Refs. [21–29].

In this paper, K^{*0} denotes a vector $K^{*0}(892)$ meson, which is reconstructed in the $K^+\pi^-$ final state experimentally by selecting candidates within 100 MeV$/c^2$ of the mass [30,31]. In the LHCb experiment, however, no attempt is made to separate the vector K^{*0} from the S wave or other broad contributions which may present in the selected $K^+\pi^-$ pair [14]. Fortunately, the S-wave fraction contribution to the $B^0 \to \bar{K}^{*0}\mu^+\mu^-$ mode has been measured by the LHCb and found to be small [13]. For the B_s case, the S-wave contamination of the $B_s^0 \to \bar{K}^{*0}\mu^+\mu^-$ decay is also unknown now and assumed to be small compared to that of the $B^0 \to \bar{K}^{*0}\mu^+\mu^-$ decay. Specifically, the S-wave fraction of $F_S(\bar{B}^0 \to \bar{K}^{*0}\mu^+\mu^-) = (3.4 \pm 0.8)\%$ in the $K^+\pi^-$ system [20]. Theoretically, the authors of Ref. [32] found the S-wave contribution will modify differential decay widths by about 10% in the process of $\bar{B}^0 \to K^-\pi^+\ell^+\ell^-$.

Analogous to the ratios R_K and R_{K^*} for $B \to K^{(*)}l^+l^-$ decays as defined in Refs. [1–14], we can define the similar ratios of the BRs $R_{s,K}^{e\mu}$ and $R_{s,K^*}^{e\mu}$ for the $\bar{B}_s \to K^{(*)}\ell^+\ell^-$ decays:

$$R_{s,K^{(*)}}^{e\mu} = \frac{\mathcal{B}(\bar{B}_s \to K^{(*)}\mu^+\mu^-)}{\mathcal{B}(\bar{B}_s \to K^{(*)}e^+e^-)}. \quad (3)$$

Similarly, we can also define the ratios $R_{s,K}^{\mu\tau}$ and $R_{s,K^*}^{\mu\tau}$ in the following form:

$$R_{s,K^{(*)}}^{\mu\tau} = \frac{\mathcal{B}(\bar{B}_s \to K^{(*)}\tau^+\tau^-)}{\mathcal{B}(\bar{B}_s \to K^{(*)}\mu^+\mu^-)}. \quad (4)$$

These new ratios $R_{s,K^{(*)}}^{e\mu}$ and $R_{s,K^{(*)}}^{\mu\tau}$, together with the ratios R_K and R_{K^*}, can help us to examine the $b \to (s,d)\ell^+\ell^-$ transitions in great details.

Unlike the well-studied $B \to K^{(*)}\ell^+\ell^-$ decays, the semileptonic $\bar{B}_s \to K^{(*)}\ell^+\ell^-$ decays have not caught much attention partially due to their lower branching ratios and the lack of the relevant experimental measurements. In recent years, these decays have been studied by several authors, for example, in Refs. [26–29], and the first measured branching ratio as listed in Eq. (2) was reported last year by the LHCb Collaboration [20]. Besides the measurements for the branching ratios, a precise angular reconstruction of the polarized K^* in $\bar{B}_s \to K^{(*)}\ell^+\ell^-$ decays was discussed in Ref. [8]. Recently, the predictions of several angular observables for the $\bar{B}_s \to K^*\ell^+\ell^-$ decays were provided using the light-cone sum rule (LCSR) and the lattice QCD method in Ref. [29].

By using the perturbative QCD (PQCD) factorization approach [33–35], the semileptonic $\bar{B}_s \to K\ell^+\ell^+$ decays have been studied by us in a previous paper [26]. We considered the next-to-leading order (NLO) contributions known at 2012 and presented our PQCD predictions of the branching ratios:

$$\mathcal{B}(\bar{B}_s^0 \to K^0\ell^+\ell^-) = (1.63^{+0.73}_{-0.58}) \times 10^{-8}, \quad l = (e,\mu), \quad (5)$$

$$\mathcal{B}(\bar{B}_s^0 \to K^0\tau^+\tau^-) = (0.43^{+0.18}_{-0.15}) \times 10^{-8}. \quad (6)$$

In this paper, we will make a systematic study for the semileptonic decays $\bar{B}_s \to (K, K^*)\ell^+\ell^-$ with $l = (e,\mu,\tau)$, and present the theoretical predictions of many new physical observables:

(1) For $\bar{B}_s \to K\ell^+\ell^-$ decays, besides the branching ratios, we also calculate their forward-backward (FB) asymmetry $\mathcal{A}_{FB}(q^2)$, the longitudinal lepton polarization asymmetry $P_L(q^2)$, the direct CP asymmetry $\mathcal{A}_{CP}$, and the ratios $R_{s,K}^{e\mu}$ and $R_{s,K}^{\mu\tau}$.

(2) For $\bar{B}_s \to K^*\ell^+\ell^-$ decays, we treat them as a four body decay $\bar{B}_s \to K^*(\to K\pi)\ell^+\ell^-$ described by four kinematic variables: the lepton invariant mass squared q^2 and three angles $(\theta_{K^*}, \theta_\ell, \phi)$. We define and calculate the full angular decay distributions, the transverse amplitudes, the partially integrated decay amplitudes over the angles $(\theta_{K^*}, \theta_\ell, \phi)$, the FB asymmetry $\mathcal{A}_{FB}(q^2)$, the K^* polarization fraction $R_{L,T}(q^2)$ and the longitudinal lepton polarization asymmetry $P_L(q^2)$, and the ratios $R_{s,K^*}^{e\mu}$ and $R_{s,K^*}^{\mu\tau}$. Since we do not know how to calculate the possible S-wave or other broad contributions related with the reconstruction of the $K\pi$ pair [13,20], we add a 10% uncertainty to the PQCD predictions of the branching ratios as an additional theoretical error [32], but neglect it in the calculations for other ratios due to the strong cancellation.

(3) We use both the PQCD factorization approach and the "PQCD + Lattice" approach to determine the values and their q^2 dependence of the $\bar{B}_s \to K^{(*)}$ transition form factors. We use the Bourrely-Caprini-Lellouch (BCL) parametrization method [36,37] to make the extrapolation for all form factors from the low-q^2 region to $q^2_{\max}$. We will calculate the branching ratios and all other physical observables using the PQCD approach and the PQCD + Lattice

approach, respectively, and compare the theoretical predictions obtained based on different models.

The paper is organized as follows: In Sec. II, we give a short review for the kinematics of the $\bar{B}_s \to K^{(*)}\ell^+\ell^-$ decays including the distribution amplitudes of B_s and $K^{(*)}$ mesons. Section III is devoted to the theoretical framework including the Hamiltonian and transition form factors based on the PQCD k_T factorization formalism. In Sec. IV, we list all the observables for both types of decays considered in this paper. Section V contains the numerical results of relevant observables and some phenomenological discussions. We conclude and summarize in the last section.

II. KINEMATICS AND THE WAVE FUNCTIONS

We discuss the kinematics of these decays in the large-recoil (low-q^2) region, where the PQCD factorization approach is applicable to the considered semileptonic decays involving $K^{(*)}$ as the final state meson. In the rest frame of $\bar{B}_s^0$ meson, we define the $\bar{B}_s^0$ meson momentum p_1, the $K^{(*)}$ momentum p_2 in the light-cone coordinates, as in Ref. [38]

$$p_1 = \frac{m_{B_s}}{\sqrt{2}}(1,1,0_\perp), \qquad p_2 = \frac{r m_{B_s}}{\sqrt{2}}(\eta^+,\eta^-,0_\perp), \quad (7)$$

where the mass ratio $r = m_K/m_{B_s}$ or m_K^*/m_{B_s}, and the factor $\eta^\pm$ is defined in the following form:

$$\eta^\pm = \eta \pm \sqrt{\eta^2-1}, \quad \text{with} \quad \eta = \frac{1}{2r}\left[1+r^2-\frac{q^2}{m_{B_s}^2}\right], \quad (8)$$

where $q = p_1 - p_2$ is the lepton-pair four-momentum. For the final state K^* meson, its longitudinal and transverse polarization vector $\epsilon_{L,T}$ can be written as

$$\epsilon_L = \frac{1}{\sqrt{2}}(\eta^+,-\eta^-,0_\perp), \qquad \epsilon_T = (0,0,1). \quad (9)$$

The momenta of the spectator quarks in B_s and $K^{(*)}$ mesons are parametrized as

$$k_1 = \left(0, x_1\frac{m_{B_s}}{\sqrt{2}}, k_{1\perp}\right), \qquad k_2 = \frac{m_{B_s}}{\sqrt{2}}(x_2 r\eta^+, x_2 r\eta^-, k_{2\perp}). \quad (10)$$

We make the approximation in the small $k_\perp$.

For the $\bar{B}_s^0$ meson wave function, we use the same parametrizations as in Refs. [26,39]

$$\Phi_{B_s} = \frac{i}{\sqrt{2N_c}}(\not{p}_{B_s} + m_{B_s})\gamma_5\phi_{B_s}(k_1). \quad (11)$$

Here, only the contribution of the Lorentz structure $\phi_{B_s}(k_1)$ is taken into account, since the contribution of the second Lorentz structure $\bar{\phi}_{B_s}$ is numerically small and has been neglected. We adopted the B_s-meson distribution amplitude that was the same as the B meson in the $SU(3)_f$ limit widely used in the PQCD approach

$$\phi_{B_s}(x,b) = N_{B_s}x^2(1-x)^2\exp\left[-\frac{m_{B_s}^2x^2}{2\omega_{B_s}^2}-\frac{1}{2}(\omega_{B_s}b)^2\right]. \quad (12)$$

In order to analyze the uncertainties of theoretical predictions induced by the inputs, one usually takes $\omega_{B_s} = 0.50 \pm 0.05$ GeV for the B_s^0 meson. The normalization factor N_{B_s} depends on the values of the shape parameter ω_{B_s} and the decay constant f_{B_s} and is defined through the normalization relation: $\int_0^1 dx\,\phi_{B_s}(x,b=0) = f_{B_s}/(2\sqrt{6})$ [26].

For the pseudoscalar K meson, the wave function can be chosen as the same one in Ref. [40]:

$$\Phi_K(p,x) \equiv \frac{i}{\sqrt{6}}\gamma_5[\not{p}_K\phi_K^A(x) + m_0^K\phi_K^p(x) + \zeta m_0^K(\not{n}\not{v}-1)\phi_K^T(x)], \quad (13)$$

where m_0^K and p are the chiral mass and the momentum of the meson K. The parameter $\zeta = 1$ or -1 when the momentum fraction of the quark (antiquark) of the meson is set to be x. The distribution amplitudes (DAs) of the kaon meson can be found easily in Refs. [41–44]:

$$\phi_K^A(x) = \frac{3f_K}{\sqrt{6}}x(1-x)[1 + a_1^K C_1^{3/2}(t) + a_2^K C_2^{3/2}(t) + a_4^K C_4^{3/2}(t)], \quad (14)$$

$$\phi_K^p(x) = \frac{f_K}{2\sqrt{6}}\left\{1 + \left(30\eta_3 - \frac{5}{2}\rho_K^2\right)C_2^{1/2}(t) - 3\left[\eta_3\omega_3 + \frac{9}{20}\rho_K^2(1+6a_2^K)C_4^{1/2}(t)\right]\right\}, \quad (15)$$

$$\phi_K^T(x) = \frac{f_K(1-2x)}{2\sqrt{6}}\left\{1 + 6\left[5\eta_3 - \frac{1}{2}\eta_3\omega_3 - \frac{7}{20}\rho_K^2 - \frac{3}{5}\rho_K^2 a_2^K\right](1-10x+10x^2)\right\}, \quad (16)$$

where $t = 2x-1$, f_K is the decay constant of the kaon meson and $\rho_K = m_K/m_K^0$ is the mass ratio. The Gegenbauer moments and other parameters are [41–44]

$$a_1^K = 0.06 \pm 0.03, \qquad a_2^K = 0.25 \pm 0.15, \qquad a_4^K = -0.015, \qquad \eta_3 = 0.015, \qquad \omega = -3.0. \quad (17)$$

The Gegenbauer polynomials that appeared in Eqs. (14) and (15) are of the following form [41–44]:

$$C_1^{3/2}(t)=3t,\qquad C_2^{1/2}(t)=\frac{1}{2}(3t^2-1),\qquad C_2^{3/2}(t)=\frac{3}{2}(5t^2-1),$$
$$C_4^{1/2}(t)=\frac{1}{8}(3-30t^2+35t^4),\qquad C_4^{3/2}(t)=\frac{15}{8}(1-14t^2+21t^4). \tag{18}$$

For the light vector meson K^*, the longitudinal and transverse polarization components can provide the contribution. Here we adopt the wave functions of the vector K^* as in Ref. [44]:

$$\Phi^{\parallel}_{K^*}(p,\epsilon_L)=\frac{i}{\sqrt{6}}[\not\epsilon_L m_{K^*}\phi_{K^*}(x)+\not\epsilon_L\not p\phi^t_{K^*}(x)+m_{K^*}\phi^s_{K^*}(x)], \tag{19}$$

$$\Phi^{\perp}_{K^*}(p,\epsilon_T)=\frac{i}{\sqrt{6}}[\not\epsilon_T m_{K^*}\phi^v_{K^*}(x)+\not\epsilon_T\not p\phi^T_{K^*}(x)+m_{K^*}i\epsilon_{\omega\nu\rho\sigma}\gamma_5\gamma^\omega\epsilon_T^\nu n^\rho v^\sigma\phi^a_{K^*}(x)], \tag{20}$$

where p and m_{K^*} are the momentum and the mass of the K^* meson, and ϵ_L and ϵ_T correspond to the longitudinal and transverse polarization vectors of the vector meson, respectively. The ϕ_{K^*} and $\phi^T_{K^*}$ in Eqs. (19) and (20) are the twist-two DAs [44]:

$$\phi_{K^*}(x)=\frac{3f_{K^*}}{\sqrt{6}}x(1-x)[1+a^{\parallel}_{1K^*}C_1^{3/2}(t)+a^{\parallel}_{2K^*}C_2^{3/2}(t)], \tag{21}$$

$$\phi^T_{K^*}(x)=\frac{3f^T_{K^*}}{\sqrt{6}}x(1-x)[1+a^{\perp}_{1K^*}C_1^{3/2}(t)+a^{\perp}_{2K^*}C_2^{3/2}(t)], \tag{22}$$

where f_{K^*} and $f^T_{K^*}$ are the longitudinal and transverse components of the decay constants. The Gegenbauer moments in Eqs. (19) and (20) are the same ones as those in Ref. [44]:

$$a^{\parallel}_{1K^*}=0.03\pm0.02,\qquad a^{\parallel}_{2K^*}=0.11\pm0.09,$$
$$a^{\perp}_{1K^*}=0.04\pm0.03,\qquad a^{\perp}_{2K^*}=0.10\pm0.08. \tag{23}$$

The twist-three DAs $\phi^{s,t}_{K^*}$ and $\phi^{v,a}_{K^*}$ in Eqs. (19) and (20) are defined with the asymptotic form as in Ref. [44]:

$$\phi^t_{K^*}=\frac{3f^T_{K^*}}{2\sqrt{6}}t^2,\qquad \phi^s_{K^*}=\frac{3f^T_{K^*}}{2\sqrt{6}}(-t),\qquad \phi^v_{K^*}=\frac{3f_{K^*}}{8\sqrt{6}}(1+t^2),\qquad \phi^a_{K^*}=\frac{3f_{K^*}}{4\sqrt{6}}(-t), \tag{24}$$

III. THEORETICAL FRAMEWORK

A. Effective Hamiltonian for $b\to d\ell^+\ell^-$ decays

For the considered $b\to d\ell^+\ell^-$ transitions, the effective Hamiltonian in the framework of the SM can be written in the following form [29,45–47]:

$$\mathcal{H}_{\rm eff}=-\frac{G_F}{\sqrt{2}}V_{tb}V^*_{td}\Big\{C_1(\mu)\mathcal{O}^c_1(\mu)+C_2(\mu)\mathcal{O}^c_2(\mu)+\sum_{i=3}^{10}C_i(\mu)\mathcal{O}_i(\mu)$$
$$+\lambda_u[C_1(\mu)(\mathcal{O}^c_1(\mu)-\mathcal{O}^u_1(\mu))+C_2(\mu)(\mathcal{O}^c_2(\mu)-\mathcal{O}^u_2(\mu))]\Big\}, \tag{25}$$

where $G_F=1.16638\times10^{-5}$ GeV^{-2} is the Fermi constant, $\lambda_u=V_{ub}V^*_{ud}/(V_{tb}V^*_{td})$ is a ratio of the CKM elements, and $C_i(\mu)$ and $\mathcal{O}_i(\mu)$ are the Wilson coefficients and the four-fermion operators at the renormalization scale μ. In the SM, a suitable basis of the operators $\mathcal{O}_i(\mu)$ for the $b\to d\ell^+\ell^-$ transition is given by the current-current operators $\mathcal{O}^{u,c}_{1,2}$, the QCD penguin operators $\mathcal{O}_{3-6}$, the electromagnetic penguin operator $\mathcal{O}_7$, and the chromomagnetic penguin operator $\mathcal{O}_8$, as well as the semileptonic operators $\mathcal{O}_{9,10}$:

$$\mathcal{O}_1^c = (\bar{d}_\alpha c_\beta)_{V-A}(\bar{c}_\beta b_\alpha)_{V-A}, \qquad \mathcal{O}_2^c = (\bar{d}_\alpha c_\alpha)_{V-A}(\bar{c}_\beta b_\beta)_{V-A},$$
$$\mathcal{O}_1^u = (\bar{d}_\alpha u_\beta)_{V-A}(\bar{u}_\beta b_\alpha)_{V-A}, \qquad \mathcal{O}_2^u = (\bar{d}_\alpha u_\alpha)_{V-A}(\bar{u}_\beta b_\beta)_{V-A},$$
$$\mathcal{O}_3 = (\bar{d}_\alpha b_\alpha)_{V-A}\sum_q (\bar{q}_\beta q_\beta)_{V-A}, \qquad \mathcal{O}_4 = (\bar{d}_\alpha b_\beta)_{V-A}\sum_q (\bar{q}_\beta q_\alpha)_{V-A},$$
$$\mathcal{O}_5 = (\bar{d}_\alpha b_\alpha)_{V-A}\sum_q (\bar{q}_\beta q_\beta)_{V+A}, \qquad \mathcal{O}_6 = (\bar{d}_\alpha b_\beta)_{V-A}\sum_q (\bar{q}_\beta q_\alpha)_{V+A},$$
$$\mathcal{O}_7 = \frac{em_b}{8\pi^2}\bar{d}\sigma^{\mu\nu}(1+\gamma_5)bF_{\mu\nu}, \qquad \mathcal{O}_8 = \frac{gm_b}{8\pi^2}\bar{d}\sigma^{\mu\nu}T^a(1+\gamma_5)bG^a_{\mu\nu},$$
$$\mathcal{O}_9 = \frac{\alpha_{\rm em}}{2\pi}(\bar{d}\gamma^\mu(1-\gamma_5)b)(\bar{\ell}\gamma_\mu\ell), \qquad \mathcal{O}_{10} = \frac{\alpha_{\rm em}}{2\pi}(\bar{d}\gamma^\mu(1-\gamma_5)b)(\bar{\ell}\gamma_\mu\gamma_5\ell), \tag{26}$$

where T^a denotes the generators of the $SU(3)_C$ group and m_b is the running b-quark mass in the $\overline{\rm MS}$ scheme; $F_{\mu\nu}$ and $G^a_{\mu\nu}$ are the electromagnetic and chromomagnetic tensors, respectively. The labels $V \pm A$ refer to the Lorentz structure $\gamma_\mu(1 \pm \gamma_5)$. In Fig. 1, we show the typical Feynman diagrams for the semileptonic decays $\bar{B}_s^0 \to K^{(*)}l^+l^-$ in the PQCD approach. The dominant contribution to the $b \to d\ell^+\ell^-$ transitions is given by $\mathcal{O}_7$ and $\mathcal{O}_{9,10}$, as well as $\mathcal{O}_{1,2}^{u,c}$. The operator $\mathcal{O}_7$ corresponds to the γ-penguin diagram, as shown in Fig. 2(a). The operators $\mathcal{O}_{9,10}$ describe the sum of the contributions from the Z and γ penguin in Fig. 2(a) and the W box diagrams in Fig. 2(b). The current-current operators $\mathcal{O}_{1,2}^{u,c}$ involve a long-distance contribution, which originates in the real $u\bar{u}$, $d\bar{d}$, and $c\bar{c}$ intermediate states, namely, the (ρ, ω, ϕ) and J/ψ family in Fig. 2(c), coupled to the lepton pair via the virtual photon. This contribution is proportional to C_9 and can be absorbed into an effective Wilson coefficient $C_9^{\rm eff}$ [48].

Here we neglect the contribution from the subleading chromomagnetic penguin, and the quark-loop and annihilation diagrams because these effects are highly suppressed [29]. Hence, the decay amplitude for $b \to dl^+l^-$ loop transition can be decomposed as

$$\mathcal{A}(b \to dl^+l^-) = \frac{G_F}{2\sqrt{2}}\frac{\alpha_{\rm em}}{\pi}V_{tb}V_{td}^*\Big\{C_9^{\rm eff}(q^2)[\bar{d}\gamma_\mu(1-\gamma_5)b][\bar{l}\gamma^\mu l] + C_{10}[\bar{d}\gamma_\mu(1-\gamma_5)b][\bar{l}\gamma^\mu\gamma_5 l]$$
$$- 2m_b C_7^{\rm eff}\left[\bar{d}i\sigma_{\mu\nu}\frac{q^\nu}{q^2}(1+\gamma_5)b\right][\bar{l}\gamma^\mu l]\Big\}, \tag{27}$$

where $C_7^{\rm eff}(\mu)$ and $C_9^{\rm eff}(\mu)$ are the effective Wilson coefficients, defined as in Refs. [26,49]

$$C_7^{\rm eff}(\mu) = C_7(\mu) + C'_{b\to d\gamma}(\mu), \tag{28}$$

$$C_9^{\rm eff}(\mu, q^2) = C_9(\mu) + Y_{\rm pert}(\hat{s}) + Y_{\rm res}(q^2). \tag{29}$$

The analytic expressions for all Wilson coefficients in the NLO approximation can be found easily in Ref. [50]. The numerical values of the NLO Wilson coefficients $C_i(\mu)$ at three different renormalization scales

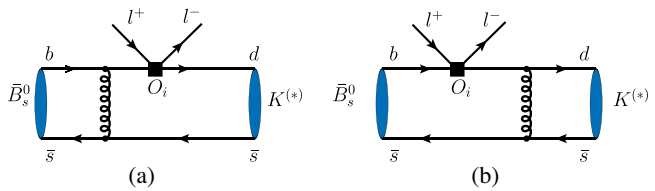

FIG. 1. The typical Feynman diagrams for the semileptonic decays $\bar{B}_s^0 \to K^{(*)}\ell^+\ell^-$ in the PQCD approach with the FCNC contributions due to the operators O_i as defined in Eq. (26) and denoted as black squares in this figure.

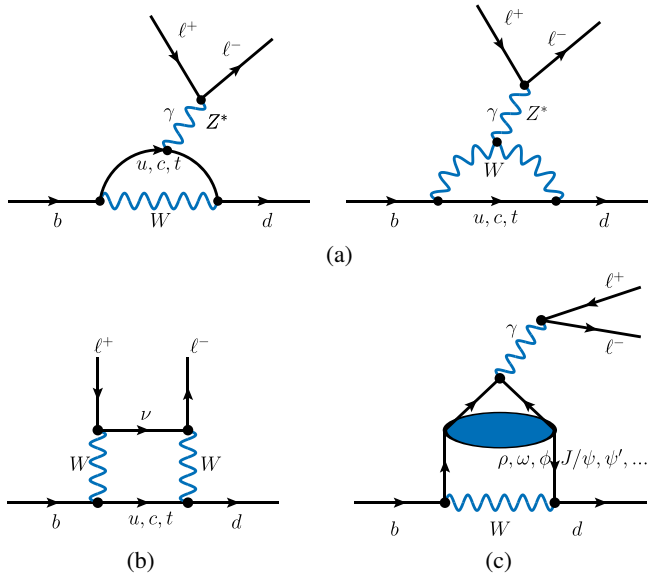

FIG. 2. Typical Feynman loop diagrams: the γ penguin (a) with $\mathcal{O}_7$, the $z(\gamma)$ penguin (a) and W box (b) with $\mathcal{O}_{9,10}$, and the loops (c) with $\mathcal{O}_{1,2}^{u,c}$.

TABLE I. The values of the Wilson coefficients $C_i(\mu)$ in NLO level at three different renormalization scales $\mu = (m_b/2, m_b, 3m_b/2)$.

$\mu\backslash C_i(\mu)$	C_1	C_2	$C_3(\%)$	$C_4(\%)$	$C_5(\%)$	$C_6(\%)$	C_7	C_8	C_9	C_{10}
$m_b/2$	−0.276	1.131	2.005	−4.845	1.375	−5.841	−0.329	−0.165	4.450	−4.410
m_b	−0.175	1.076	1.258	−3.279	1.112	−3.634	−0.302	−0.148	4.232	−4.410
$3m_b/2$	−0.129	1.053	0.966	−2.608	0.964	−2.786	−0.287	−0.139	4.029	−4.410

$\mu = (m_b/2, m_b, 3m_b/2)$ are listed in Table I. Note that the Wilson coefficient C_{10} is independent of the μ scale and $C_9(\mu)$ is relatively sensitive to the choice of μ.

The term $C'_{b\to d\gamma}$ in Eq. (28) is the absorptive part of $b \to d\gamma$ and was given in Ref. [49]

$$C'_{b\to d\gamma}(\mu) = i\alpha_s\left\{\frac{2}{9}\eta^{14/23}[G_I(x_t) - 0.1687] - 0.03C_2(\mu)\right\}, \tag{30}$$

where $\eta = \alpha_s(m_W)/\alpha_s(\mu)$, $x_t = m_t^2/m_W^2$ and

$$G_I(x_t) = \frac{x_t(x_t^2 - 5x_t - 2)}{8(x_t - 1)^3} + \frac{3x_t^2 \ln x_t}{4(x_t - 1)^4}. \tag{31}$$

Besides the ordinary Wilson coefficient $C_9(\mu)$, the effective Wilson coefficient $C_9^{\rm eff}(q^2)$ in Eq. (29) also contains two additional effective terms $Y_{\rm pert}(\hat{s})$ and $Y_{\rm res}(q^2)$. The term $Y_{\rm pert}(\hat{s})$ describes the short distance contribution from the soft-gluon emission and the one-loop contribution of the four-quark operators $\mathcal{O}_1 - \mathcal{O}_6$. The term $Y_{\rm res}(q^2)$ includes the contributions of the virtual resonances described by the Breit-Wigner form prescribed in Refs. [47,51–54].

$$\begin{aligned} Y_{\rm pert}(\hat{s}) = {} & 0.124\omega(\hat{s}) + g(\hat{m}_c, \hat{s})C_0 + \lambda_u[g(\hat{m}_c, \hat{s}) - g(\hat{m}_u, \hat{s})](3C_1 + C_2) \\ & - \frac{1}{2}g(\hat{m}_d, \hat{s})(C_3 + 3C_4) - \frac{1}{2}g(\hat{m}_b, \hat{s})(4C_3 + 4C_4 + 3C_5 + C_6) \\ & + \frac{2}{9}(3C_3 + C_4 + 3C_5 + C_6), \end{aligned} \tag{32}$$

$$\begin{aligned} Y_{\rm res}(q^2) = {} & -\frac{3\pi}{\alpha_{\rm em}^2}\left[C_0 \cdot \sum_{V=J/\Psi,\Psi'\ldots} \frac{m_V\mathcal{B}(V \to l^+l^-)\Gamma_{\rm tot}^V}{q^2 - m_V^2 + im_V\Gamma_{\rm tot}^V}\right. \\ & \left. - \lambda_u g(\hat{m}_u, \hat{s})(3C_1 + C_2) \cdot \sum_{V=\rho,\omega,\phi} \frac{m_V\mathcal{B}(V \to l^+l^-)\Gamma_{\rm tot}^V}{q^2 - m_V^2 + im_V\Gamma_{\rm tot}^V}\right], \end{aligned} \tag{33}$$

where $C_0 = 3C_1 + C_2 + 3C_3 + C_4 + 3C_5 + C_6$, $\hat{s} = q^2/m_b^2$, and $\hat{m}_q = m_q/m_b$. In the above expressions, $\omega(\hat{s})$ is the soft-gluon correction to the matrix element of operator $\mathcal{O}_9$ and was given in Refs. [47,55]

$$\begin{aligned} \omega(\hat{s}) = {} & -\frac{2}{9}\pi^2 + \frac{4}{3}\int_0^{\hat{s}} \frac{\ln(1-u)}{u}du - \frac{2}{3}\ln(\hat{s})\ln(1-\hat{s}) - \frac{5 + 4\hat{s}}{3(1 + 2\hat{s})}\ln(1-\hat{s}) \\ & - \frac{2\hat{s}(1+\hat{s})(1-2\hat{s})}{3(1-\hat{s})^2(1+2\hat{s})}\ln\hat{s} + \frac{5 + 9\hat{s} - 6\hat{s}^2}{6(1-\hat{s})(1+2\hat{s})}. \end{aligned} \tag{34}$$

The loop coefficient functions $g(\hat{m}_q, \hat{s})$ in Eqs. (32) and (33) describe the one-loop $(q\bar{q})$ contributions to the four-quark operators $\mathcal{O}_1 - \mathcal{O}_6$, and can be written as the well-known expression [56–59]:

$$g(\hat{m}_q, \hat{s}) = -\frac{8}{9}\ln(\hat{m}_q) + \frac{8}{27} + \frac{4}{9}x - \frac{2}{9}(2 + x)\sqrt{|1 - x|} \times \begin{cases} 2\arctan\frac{1}{\sqrt{x-1}} & , x > 1 \\ \ln\left|\frac{1+\sqrt{1-x}}{1-\sqrt{1-x}}\right| - i\pi & , x < 1, \end{cases} \tag{35}$$

where $x \equiv 4\hat{m}_q^2/\hat{s}$.

In Ref. [59], the authors employed the dispersion approach to compute the charm-loop effect in a form of the correction to the Wilson coefficient C_9. By fitting the whole dispersion relation to the operator-product expansion (OPE) result at $q^2 \ll 4m_c^2$, the authors found that there exists a destructive interference between the J/ψ and $\psi(2S)$ states. According to their opinion, a reliable prediction for the charm-loop effect above $\psi(2S)$ based on QCD is hard to make. Although the actual effect,

TABLE II. The masses, decay widths and branching fractions of the dilepton decays of the vector charmonium states [30].

V	Mass [GeV]	$\Gamma^V_{\rm tot}$ [MeV]	$\mathcal{BR}(V \to l^+l^-)$ with $l = e, \mu$
$\rho(770)$	0.775	149.1	4.63×10^{-5}
$\omega(782)$	0.782	8.490	7.38×10^{-5}
$\phi(1020)$	1.019	4.249	2.92×10^{-4}
$J/\psi(1S)$	3.096	0.093	5.96×10^{-2}
$\psi(2S)$	3.686	0.294	7.96×10^{-3}
$\psi(3770)$	3.773	27.2	9.60×10^{-6}
$\psi(4040)$	4.039	80	1.07×10^{-5}
$\psi(4160)$	4.191	70	6.90×10^{-6}
$\psi(4415)$	4.421	62	9.40×10^{-6}

depending on the interference of many charmonium states, cannot be reliably constrained by OPE, it could be considered as small in this region.

The term $Y_{\rm res}$ in Eq. (33) denotes the long-distance resonance contributions from those $B_s \to K^{(*)}V \to K^{(*)}(V \to \ell^+\ell^-)$ transitions, where V stands for the possible intermediate resonance states decaying to lepton pairs:

(1) The charmless light vector mesons $V = (\rho, \omega, \phi)$. The kinematic region where the light resonances (ρ, ω, ϕ) contribute is typically not excluded from the experimental analyses because their effects on branching fractions and other physical observables might be substantial [60].

(2) The $c\bar{c}$ charmonia $V_{c\bar{c}} = \psi(1S, 2S, 3770, 4040, 4160, 4415)$. The two lowest charmonium states $\psi(1S)$ and $\psi(2S)$ (i.e., J/ψ and ψ'), whose masses are below the open charm threshold ($D\bar{D}$), have tiny width and can induce large breaking of quark-hadron duality. Hence, the narrow charmonia resonance regions are routinely rejected in the theoretical and experimental analysis. For the four higher charmonium resonances, however, they are broad and overlapping throughout the high-q^2 regions. One usually makes the integration over the full high-q^2 range.

As reported in Ref. [61], a resonance above $\psi(2S)$ compatible with the $\psi(4160)$ has been observed by LHCb in the $B \to K\mu^+\mu^-$ decay. Consequently, nearly all available contributions about the $J^{PC} = 1^{--}$ charmonium resonances above the open charm threshold should be taken into account [62]. In Table II, we list the properties of all considered intermediate resonance states: their mass, width, and branching fractions of the leptonic decay channel $V \to l^+l^-$ [30]. For the case $\ell = \tau$, only the fraction of $J/\psi(2S) \to \tau^+\tau^-$ does not vanish, which equals 3.1×10^{-3} from Ref. [30].

B. $B_s \to K, K^*$ transition form factors

The $B_s \to K$ transition can be induced by the vector current V^μ and the tensor currents $T^{\mu\nu}$:

$$\langle K(p_2)|V^\mu|B_s(p_1)\rangle = f_1(q^2)p_1^\mu + f_2(q^2)p_2^\mu, \quad (36)$$

$$\langle K(p_2)|T^{\mu\nu}|B_s(p_1)\rangle = i\frac{2}{m_{B_s}+m_K}[p_2^\mu q^\nu - q^\mu p_2^\nu]F_T(q^2), \quad (37)$$

where $V^\mu = \bar{d}\gamma^\mu b$ and $T^{\mu\nu} = \bar{d}\sigma^{\mu\nu}b$, and $q = p_1 - p_2$ is the momentum carried off by the lepton pairs and $\sigma^{\mu\nu} = i[\gamma^\mu, \gamma^\nu]/2$.

The $B_s \to K$ transition form factors $F_+(q^2)$ and $F_0(q^2)$ can be written as a combination of the auxiliary form factors $f_1(q^2)$ and $f_2(q^2)$ in Eq. (36):

$$F_+(q^2) = \frac{1}{2}[f_1(q^2) + f_2(q^2)], \quad (38)$$

$$F_0(q^2) = F_+(q^2) + \frac{1}{2}[f_1(q^2) - f_2(q^2)]\frac{q^2}{m_{B_s}^2 - m_K^2}. \quad (39)$$

We also have the relation $F_+(0) = F_0(0)$ in order to smear the pole at $q^2 = 0$.

Using the well-studied wave functions as given in Sec. II, we calculated the three $B_s \to K$ form factors $f_1(q^2)$, $f_2(q^2)$, and $F_T(q^2)$ in the PQCD factorization approach:

$$\begin{aligned} f_1(q^2) = {} & 16\pi m_{B_s}^2 C_F \int dx_1 dx_2 \int b_1 db_1 b_2 db_2 \phi_{B_s}(x_1) \\ & \times \left\{ \left[-x_2 r^2 \phi_K^A(x_2) + r_0 \phi_K^P(x_2) - \frac{\eta + 2x_2 r}{\sqrt{\eta^2 - 1}} r_0 \phi_K^T(x_2) \right] \cdot H_1(t_1) \right. \\ & + \left[\left(x_1(\eta + \sqrt{\eta^2 - 1}) - r + \frac{x_1}{2\sqrt{\eta^2 - 1}} \right) r\phi_K^A(x_2) \right. \\ & \left. \left. - x_1 \left(1 + \frac{\eta}{\sqrt{\eta^2 - 1}} \right) r_0 \phi_K^P(x_2) \right] \cdot H_2(t_2) \right\}, \end{aligned} \quad (40)$$

$$f_2(q^2) = 16\pi m_{B_s}^2 C_F \int dx_1 dx_2 \int b_1 db_1 b_2 db_2 \phi_{B_s}(x_1) \times \left\{ \left[(1 + x_2 r\eta)\phi_K^A(x_2) - 2x_2 r_0 \phi_K^P(x_2) - \frac{1 - 2x_2 r\eta}{r\sqrt{\eta^2 - 1}} r_0 \phi_K^T(x_2) \right] \cdot H_1(t_1) + \left[-\frac{x_1}{2} \left(1 + \frac{\eta}{\sqrt{\eta^2 - 1}} \right) \phi_K^A(x_2) + \left(2 + \frac{x_1}{r\sqrt{\eta^2 - 1}} \right) r_0 \phi_K^P(x_2) \right] \cdot H_2(t_2) \right\}, \tag{41}$$

$$F_T(q^2) = 8\pi m_{B_s}^2 C_F (1 + r) \int dx_1 dx_2 \int b_1 db_1 b_2 db_2 \phi_{B_s}(x_1) \times \left\{ \left[\phi_K^A(x_2) - x_2 r_0 \phi_K^P(x_2) - \frac{1 + x_2 r\eta}{r\sqrt{\eta^2 - 1}} r_0 \phi_K^T(x_2) \right] \cdot H_1(t_1) + \left[-\frac{x_1}{2} \left(1 + \frac{\eta}{\sqrt{\eta^2 - 1}} \right) \phi_K^A(x_2) + \left(2 + \frac{x_1}{r\sqrt{\eta^2 - 1}} \right) r_0 \phi_K^P(x_2) \right] \cdot H_2(t_2) \right\}. \tag{42}$$

where $C_F = 4/3$ is a color factor, $r_0 = m_K^0/m_{B_s}$, $r = m_k/m_{B_s}$, η is defined in Eq. (8), and the function $H_i(t_i)$ in the following form:

$$H_i(t_i) = h_i(x_1, x_2, b_1, b_2) \cdot \alpha_s(t_i) \exp[-S_{ab}(t_i)], \quad \text{for } i = (1, 2). \tag{43}$$

The explicit expressions of the hard functions $h_{1,2}(x_1, x_2, b_1, b_2)$, the hard scales $t_{1,2}$, and the Sudakov factors $S_{ab}(t_i)$ will be given in the Appendix.

For the vector meson K^* with polarization vector ϵ^*, the relevant form factors for $B_s \to K^*$ transitions are $V(q^2)$ and $A_{0,1,2}(q^2)$ of the vector and axial-vector currents, and $T_{1,2,3}(q^2)$ of the tensor currents. In the PQCD factorization approach, these seven form factors of $B_s \to K^* \ell^+ \ell^-$ decays can be calculated and written in the following form:

$$V(q^2) = 8\pi m_{B_s}^2 C_F (1 + r) \int dx_1 dx_2 \int b_1 db_1 b_2 db_2 \phi_{B_s}(x_1) \times \left\{ \left[-x_2 r \phi_{K^*}^v(x_2) + \phi_{K^*}^T(x_2) + \frac{1 + x_2 r\eta}{\sqrt{\eta^2 - 1}} \phi_{K^*}^a(x_2) \right] \cdot H_1(t_1) + \left[\left(r + \frac{x_1}{2\sqrt{\eta^2 - 1}} \right) \phi_{K^*}^v(x_2) - \frac{x_1 - 2r\eta}{2\sqrt{\eta^2 - 1}} \phi_{K^*}^a(x_2) \right] \cdot H_2(t_2) \right\}, \tag{44}$$

$$A_0(q^2) = 8\pi m_{B_s}^2 C_F \int dx_1 dx_2 \int b_1 db_1 b_2 db_2 \phi_{B_s}(x_1) \times \left\{ \left[(1 + x_2 r(2\eta - r)) \phi_{K^*}(x_2) + (1 - 2x_2) r \phi_{K^*}^t(x_2) + \frac{(1 - r\eta) - 2x_2 r(\eta - r)}{\sqrt{\eta^2 - 1}} \phi_{K^*}^s(x_2) \right] \cdot H_1(t_1) + \left[\left[\frac{x_1}{\sqrt{\eta^2 - 1}} \left(\frac{\eta + r}{2} - r\eta^2 \right) + \left(\frac{x_1}{2} - x_1 r\eta + r^2 \right) \right] \phi_{K^*}(x_2) - \left[\frac{x_1(1 - r\eta) + 2r(r - \eta)}{\sqrt{\eta^2 - 1}} - x_1 r \right] \phi_{K^*}^s(x_2) \right] \cdot H_2(t_2) \right\}, \tag{45}$$

$$A_1(q^2) = 16\pi m_{B_s}^2 C_F \frac{r}{1 + r} \int dx_1 dx_2 \int b_1 db_1 b_2 db_2 \phi_{B_s}(x_1) \times \left\{ \left[(1 + x_2 r\eta)\phi_{K^*}^v(x_2) + (\eta - 2x_2 r)\phi_{K^*}^T(x_2) + x_2 r\sqrt{\eta^2 - 1}\phi_{K^*}^a(x_2) \right] \cdot H_1(t_1) + \left[\left(r\eta - \frac{x_1}{2} \right) \phi_{K^*}^v(x_2) + \left(r\sqrt{\eta^2 - 1} + \frac{x_1}{2} \right) \phi_{K^*}^a(x_2) \right] \cdot H_2(t_2) \right\}, \tag{46}$$

$$A_2(q^2) = \frac{(1+r)^2(\eta-r)}{2r(\eta^2-1)}A_1(q^2) - 8\pi m_{B_s}^2 C_F \frac{1+r}{\eta^2-r}\int dx_1 dx_2 \int b_1 db_1 b_2 db_2 \phi_{B_s}(x_1)$$
$$\times \Big\{ \Big[[\eta(1-x_2 r^2) + r(x_2(2\eta^2-1)-1)]\phi_{K^*}(x_2) + [1+2x_2 r^2 - (1+2x_2)r\eta]\phi_{K^*}^t(x_2)$$
$$+ r(1-2x_2)\sqrt{\eta^2-1}\phi_{K^*}^s(x_2)\Big]\cdot H_1(t_1)$$
$$+ \Big[\Big[\Big(r\eta - \frac{1}{2}\Big)x_1\sqrt{\eta^2-1} - [r(r\eta - 1 - x_1\eta^2) + \frac{x_1(r+\eta)}{2}\Big]\Big]\phi_{K^*}(x_2)$$
$$+ \Big[x_1(r\eta-1) + (x_2-2)r\sqrt{\eta^2-1}\Big]\phi_{K^*}^s(x_2)]\cdot H_2(t_2)\Big\}, \tag{47}$$

$$T_1(q^2) = 8\pi m_{B_s}^2 C_F \int dx_1 dx_2 \int b_1 db_1 b_2 db_2 \phi_{B_s}(x_1) \times \Big\{ \Big[(1-2x_2) r\phi_{K^*}^v(x_2)$$
$$+ (1 + 2x_2 r\eta - x_2 r^2)\phi_{K^*}^T(x_2) + \frac{1+2x_2 r^2 - (1+2x_2)r\eta}{\sqrt{\eta^2-1}}\phi_{K^*}^a(x_2)\Big]\cdot H_1(t_1)$$
$$+ \Big[\Big[\Big(1-\frac{x_1}{2}\Big)r - \frac{x_1(r\eta-1)}{2\sqrt{\eta^2-1}}\Big]\phi_{K^*}^v(x_2) + \Big[\frac{r(\eta-r)}{\sqrt{\eta^2-1}} + \frac{x_1}{2}\Big(r + \frac{r\eta-1}{\sqrt{\eta^2-1}}\Big)\Big]\phi_{K^*}^a(x_2)\Big]\cdot H_2(t_2)\Big\}, \tag{48}$$

$$T_2(q^2) = 16\pi m_{B_s}^2 C_F \frac{r}{1-r^2}\int dx_1 dx_2 \int b_1 db_1 b_2 db_2 \phi_{B_s}(x_1)$$
$$\times \Big\{ \Big[(1-(1+2x_2)r\eta + 2x_2 r^2)\phi_{K^*}^v(x_2)$$
$$+ [x_2 r\eta(2\eta - r) - x_2 r + \eta - r]\phi_{K^*}^T(x_2) + (1-2x_2)r\sqrt{\eta^2-1}\phi_{K^*}^a(x_2)\Big]\cdot H_1(t_1)$$
$$+ \Big[\Big[\frac{x_2}{2}\Big(1 + \frac{\eta}{\sqrt{\eta^2-1}}\Big)(r\eta - 1) + \Big(r + \frac{x_1}{2\sqrt{\eta^2-1}}\Big)(\eta - r)\Big]\phi_{K^*}^v(x_2)$$
$$+ \Big[\Big(1-\frac{x_1}{2}\Big)r\sqrt{\eta^2-1} + \frac{x_1}{2}(1-r\eta)\Big]\phi_{K^*}^a(x_2)\Big]\cdot H_2(t_2)\Big\}, \tag{49}$$

$$T_3(q^2) = \frac{(1-r)^2(\eta+r)}{2r(\eta^2-1)}T_2(q^2) - 8\pi m_{B_s}^2 C_F \frac{1-r^2}{\eta^2-1}\int dx_1 dx_2 \int b_1 db_1 b_2 db_2 \phi_{B_s}(x_1)$$
$$\times \Big\{ \Big[\frac{\eta^2 - (1+2x_2)r\eta + 2x_2 r^2}{\eta - r}\phi_{K^*}(x_2) + (1 + x_2 r\eta)\phi_{K^*}^t(x_2) + x_2 r\sqrt{\eta^2-1}\phi_{K^*}^s(x_2)\Big]\cdot H_1(t_1)$$
$$+ \Big[\Big[r - \frac{x_1}{2}\Big(\eta + \sqrt{\eta^2-1}\Big)\Big]\phi_{K^*}(x_2) + \Big(x_1 + 2r\sqrt{\eta^2-1}\Big)\phi_{K^*}^s(x_2)\Big]\cdot H_2(t_2)\Big\}, \tag{50}$$

where $r = m_{K^*}/m_{B_s}$, the twist-two DAs $(\phi_{K^*}, \phi_{K^*}^T)$ and other four twist-three DAs are defined in Eqs. (19), (20), and (24), and the functions $H_{1,2}(t_{1,2})$ are the same ones as those defined in Eq. (43) for $B_s \to K$ transition, but with a replacement of $r = m_K/m_{B_s}$ by $r = m_{K^*}/m_{B_s}$.

IV. OBSERVABLES FOR $B_s \to K^{(*)}\ell^+\ell^-$ DECAYS

A. Observables for $B_s \to K\ell^+\ell^-$ decays

Within the SM operator basis, the decay amplitude of $B_s \to K\ell^+\ell^-$ decay can be written in the following form [63]:

$$\mathcal{A}(\bar{B}_s^0 \to K\ell^+\ell^-) = \frac{G_F \alpha_{em}}{\sqrt{2}\pi} V_{tb}V_{td}^*[\delta_V p_1^\mu(\bar{\ell}\gamma_\mu\ell) + \delta_A p_1^\mu(\bar{\ell}\gamma_\mu\gamma_5\ell) + \delta_P(\bar{\ell}\gamma_5\ell)] \tag{51}$$

with

$$\delta_A = C_{10} F_+(q^2),$$
$$\delta_V = C_9^{\rm eff} F_+(q^2) + C_7^{\rm eff} \frac{2(m_b - m_d)}{m_{B_s} + m_K} F_T(q^2),$$
$$\delta_P = -m_\ell C_{10} \left\{ F_+(q^2) + \frac{m_{B_s}^2 - m_K^2}{q^2} [F_+(q^2) - F_0(q^2)] \right\}, \tag{52}$$

where p_1^μ denotes the four-momentum of the B_s meson and m_ℓ is the lepton mass.

Based on the matrix elements of the operators in terms of the form factors, we obtain the double differential decay rate for $\bar{B}_s \to K\ell^+\ell^-$ with respect to q^2 and θ_ℓ with lepton flavor ℓ [64],

$$\frac{d^2\Gamma}{dq^2 d\cos\theta_\ell} = a_\ell(q^2) + b_\ell(q^2)\cos\theta_\ell + c_\ell(q^2)\cos^2\theta_\ell. \tag{53}$$

The angle θ_ℓ is defined as the angle between the $\bar{B}_s$ direction and the ℓ^- direction in the $\ell^+\ell^-$ rest frame. The corresponding angular coefficients a_ℓ, b_ℓ, and c_ℓ can be written as [63,64]

$$a_\ell(q^2) = \mathcal{N}\Big[q^2|\delta_P|^2 + \frac{\lambda}{4}(|\delta_A|^2 + |\delta_V|^2) + 4m_\ell^2 m_{B_s}^2 |\delta_A|^2 + 2m_\ell(m_{B_s}^2 - m_K^2 + q^2)\mathrm{Re}(\delta_P \delta_A^*) \Big], \tag{54}$$

$$b_\ell(q^2) = 0, \tag{55}$$

$$c_\ell(q^2) = -\frac{\mathcal{N}\lambda\beta_\ell^2}{4}(|\delta_A|^2 + |\delta_V|^2), \tag{56}$$

with the factor $\mathcal{N}$,

$$\mathcal{N} = \frac{G_F^2 \alpha_{em}^2 |V_{tb}V_{td}^*|^2}{2^9\pi^5 m_{B_s}^3} \beta_\ell \sqrt{\lambda}, \tag{57}$$

where $\beta_l = \sqrt{1 - 4\hat{m}_l^2}$ with $\hat{m}_l = m_l/\sqrt{q^2}$, $\alpha_{em} = 1/137$ is the fine structure constant, m_ℓ means the lepton mass, and $\lambda = \lambda(m_{B_s}^2, m_K^2, q^2)$ is the Källen function: $\lambda(a,b,c) = a^2 + b^2 + c^2 - 2(ab + bc + ca)$.

Integration over the polar angle θ_ℓ leads to the expression for the differential decay rate,

$$\frac{d\Gamma}{dq^2} = 2a_\ell(q^2) + \frac{2}{3}c_\ell(q^2). \tag{58}$$

We see that the linear dependence on $\cos\theta_\ell$ is lost after integration over θ_ℓ, consequently, the lepton forward-backward asymmetry $\mathcal{A}_{\rm FB}$ will also become zero,

$$\mathcal{A}_{\rm FB}(q^2) = \frac{\int_0^1 \frac{d^2\Gamma}{dq^2 d\cos\theta_\ell} d\cos\theta_\ell - \int_{-1}^0 \frac{d^2\Gamma}{dq^2 d\cos\theta_\ell} d\cos\theta_\ell}{d\Gamma/dq^2} = \frac{b_\ell(q^2)}{d\Gamma/dq^2} = 0. \tag{59}$$

Another observable of interest that we calculate is the longitudinal polarization asymmetry $P_L(q^2)$ of the leptons defined as [46]

$$P_L(q^2) = \frac{1}{d\Gamma/dq^2}\left[\frac{d\Gamma^{h_\ell=-1}}{dq^2} - \frac{d\Gamma^{h_\ell=+1}}{dq^2}\right], \tag{60}$$

where $h_\ell = +1(-1)$ implies a right-handed (left-handed) charged lepton ℓ^- in the final state. For the $\bar{B}_s \to K\ell^+\ell^-$ decay, the lepton polarization is given by [46]

$$P_L(q^2) = \frac{1}{3}\cdot\frac{G_F^2\alpha_{em}^2|V_{tb}V_{td}^*|^2}{256\pi^5 m_{B_s}^3}\cdot\frac{\beta_\ell^2\lambda^{3/2}\cdot\mathrm{Re}\{\delta_V\delta_A^*\}}{d\Gamma/dq^2}. \tag{61}$$

For the CP-conjugated mode $B_s^0 \to \bar{K}\ell^+\ell^-$, the decay amplitude and physical observables are obtained by making the substitution $\mathcal{A} \to \bar{\mathcal{A}}$, i.e., by making the complex conjugation of the CKM factor involved for the $\bar{B}_s^0$ decay modes. Analogous to Ref. [65], we also define the direct CP asymmetry of the considered $B_s \to Kl^+l^-$ decays in the following form:

$$\mathcal{A}_{CP}(q^2) = \frac{d\Gamma(\bar{B}_s \to Kl^+l^-)/dq^2 - d\bar{\Gamma}(B_s \to \bar{K}l^+l^-)/dq^2}{d\Gamma(\bar{B}_s \to Kl^+l^-)/dq^2 + d\bar{\Gamma}(B_s \to \bar{K}l^+l^-)/dq^2}. \tag{62}$$

B. Observables for $B_s \to K^*\ell^+\ell^-$

For a four body decay, $B_s \to K^*(\to \pi K)\ell^+\ell^-$, the decay distribution can be completely described in terms of four kinematic variables [7,65,66]: the lepton invariant mass squared (q^2) and three angles θ_{K^*}, θ_ℓ, and ϕ. The angle θ_{K^*} is the angle between the direction of flight of K and the B_s meson in the rest frame of K^*, θ_ℓ is the angle made by ℓ^- with respect to the B_s meson in the dilepton rest frame and ϕ is the azimuthal angle between the two planes formed by dilepton and πK. The full angular decay distribution of $\bar{B}_s \to K^*(\to \pi^- K^+)\ell^+\ell^-$ is given by [8,29,67],

$$\frac{d^4\Gamma}{dq^2 d\cos\theta_{K^*} d\cos\theta_\ell d\phi} = \frac{9}{32\pi} I(q^2, \theta_{K^*}, \theta_\ell, \phi), \tag{63}$$

where the functions $I(q^2, \theta_{K^*}, \theta_\ell, \phi)$ are of the following form [8]:

$$
\begin{aligned}
I(q^2,\theta_\ell,\theta_{K^*},\phi) &= \sum_i I_i(q^2) f_i(\theta_{K^*},\theta_\ell,\phi) \\
&= I_1^s \sin^2\theta_{K^*} + I_1^c \cos^2\theta_{K^*} + (I_2^s \sin^2\theta_{K^*} + I_2^c \cos^2\theta_{K^*})\cos 2\theta_\ell \\
&\quad + I_3 \sin^2\theta_{K^*}\sin^2\theta_\ell \cos 2\phi + I_4 \sin 2\theta_{K^*}\sin 2\theta_\ell \cos\phi \\
&\quad + I_5 \sin 2\theta_{K^*}\sin\theta_\ell \cos\phi + I_6^s \sin^2\theta_{K^*}\cos\theta_\ell + I_7 \sin 2\theta_{K^*}\sin\theta_\ell \sin\phi \\
&\quad + I_8 \sin 2\theta_{K^*}\sin 2\theta_\ell \sin\phi + I_9 \sin^2\theta_{K^*}\sin^2\theta_\ell \sin 2\phi. \qquad (64)
\end{aligned}
$$

For the CP-conjugated mode $B_s \to \bar{K}^*(\to \pi^+ K^-)\ell^+\ell^-$, the corresponding expression of the angular decay distribution is

$$
\frac{d^4\bar{\Gamma}}{dq^2 d\cos\theta_{K^*} d\cos\theta_\ell d\phi} = \frac{9}{32\pi}\bar{I}(q^2,\theta_{K^*},\theta_\ell,\phi). \qquad (65)
$$

The function $\bar{I}(q^2,\theta_{K^*},\theta_\ell,\phi)$ is obtained from Eq. (64) by the substitution [8]:

$$
I_{1,2,3,4,7} \to \bar{I}_{1,2,3,4,7}, I_{5,6,8,9} \to -\bar{I}_{5,6,8,9}, \qquad (66)
$$

where $\bar{I}_i$ are obtained by making the complex conjugation for all weak phases in I_i. The minus sign in Eq. (66) is a result of the convention that, under the previous definitions of three angles, a CP transformation interchanges the lepton and antilepton, leading to the modification $\theta_\ell \to \theta_\ell - \pi$ and $\phi \to -\phi$.

The angular coefficients I_i of the distributions in the above equation can be written in terms of the transverse amplitudes [16,68]. For the massless case there are six such complex amplitudes: $\mathcal{A}_0^{R,L}$, $\mathcal{A}_\parallel^{R,L}$, and $\mathcal{A}_\perp^{R,L}$. For the massive case, an additional complex amplitude $\mathcal{A}_t$ is required. In Table III, we show the expressions for those angular coefficients $I_i(q^2)$ and the corresponding angular factor $f_i(\theta_{K^*},\theta_\ell,\phi)$ as those defined in Refs. [16,68].

The seven transversity amplitudes $\mathcal{A}_0^{R,L}$, $\mathcal{A}_\parallel^{R,L}$, $\mathcal{A}_\perp^{R,L}$, and $\mathcal{A}_t$, in turn, can be expressed in terms of the relevant $B_s \to K^*\ell^+\ell^-$ form factors [6,8]:

$$
\mathcal{A}_\perp^{L,R} = -N_\ell\sqrt{2N_{K^*}}\sqrt{\lambda}\left[(C_9^{\rm eff} \mp C_{10})\frac{V(q^2)}{m_{B_s}+m_{K^*}} + 2\hat{m}_b C_7^{\rm eff} T_1(q^2)\right], \qquad (67)
$$

$$
\mathcal{A}_\parallel^{L,R} = N_\ell\sqrt{2N_{K^*}}[(C_9^{\rm eff} \mp C_{10})(m_{B_s}+m_{K^*})A_1(q^2) + 2\hat{m}_b C_7^{\rm eff}(m_{B_s}^2 - m_{K^*}^2)T_2(q^2)], \qquad (68)
$$

TABLE III. The explicit expressions of the angular coefficients $I_i(q^2)$ and f_i that appeared in Eq. (64).

i	$I_i(q^2)$	f_i
$1s$	$(\frac{3}{4}-\hat{m}_\ell^2)[\lvert\mathcal{A}_\parallel^L\rvert^2+\lvert\mathcal{A}_\perp^L\rvert^2+\lvert\mathcal{A}_\parallel^R\rvert^2+\lvert\mathcal{A}_\perp^R\rvert^2]+4\hat{m}_\ell^2\mathrm{Re}[\mathcal{A}_\perp^L\mathcal{A}_\perp^{R*}+\mathcal{A}_\parallel^L\mathcal{A}_\parallel^{R*}]$	$\sin^2\theta_{K^*}$
$1c$	$\lvert\mathcal{A}_0^L\rvert^2+\lvert\mathcal{A}_0^R\rvert^2+4\hat{m}_\ell^2[\lvert\mathcal{A}_t\rvert^2+2\mathrm{Re}[\mathcal{A}_0^L\mathcal{A}_0^{R*}]]$	$\cos^2\theta_{K^*}$
$2s$	$\frac{1}{4}\beta_\ell^2[\lvert\mathcal{A}_\parallel^L\rvert^2+\lvert\mathcal{A}_\perp^L\rvert^2+\lvert\mathcal{A}_\parallel^R\rvert^2+\lvert\mathcal{A}_\perp^R\rvert^2]$	$\sin^2\theta_{K^*}\cos 2\theta_\ell$
$2c$	$-\beta_\ell^2[\lvert\mathcal{A}_0^L\rvert^2+\lvert\mathcal{A}_0^R\rvert^2]$	$\cos^2\theta_{K^*}\cos 2\theta_\ell$
3	$\frac{1}{2}\beta_\ell^2[\lvert\mathcal{A}_\perp^L\rvert^2-\lvert\mathcal{A}_\parallel^L\rvert^2+\lvert\mathcal{A}_\perp^R\rvert^2-\lvert\mathcal{A}_\parallel^R\rvert^2]$	$\sin^2\theta_{K^*}\sin^2\theta_\ell\cos 2\phi$
4	$\sqrt{\frac{1}{2}}\beta_\ell^2\mathrm{Re}(\mathcal{A}_0^L\mathcal{A}_\parallel^{L*}+\mathcal{A}_0^R\mathcal{A}_\parallel^{R*})$	$\sin 2\theta_{K^*}\sin 2\theta_\ell\cos\phi$
5	$\sqrt{2}\beta_\ell\mathrm{Re}(\mathcal{A}_0^L\mathcal{A}_\perp^{L*}-\mathcal{A}_0^R\mathcal{A}_\perp^{R*})$	$\sin 2\theta_{K^*}\sin\theta_\ell\cos\phi$
$6s$	$2\beta_\ell\mathrm{Re}(\mathcal{A}_\parallel^L\mathcal{A}_\perp^{L*}-\mathcal{A}_\parallel^R\mathcal{A}_\perp^{R*})$	$\sin^2\theta_{K^*}\cos\theta_\ell$
7	$\sqrt{2}\beta_\ell\mathrm{Im}(\mathcal{A}_0^L\mathcal{A}_\parallel^{L*}-\mathcal{A}_0^R\mathcal{A}_\parallel^{R*})$	$\sin 2\theta_{K^*}\sin\theta_\ell\sin\phi$
8	$\sqrt{\frac{1}{2}}\beta_\ell^2\mathrm{Im}(\mathcal{A}_0^L\mathcal{A}_\perp^{L*}+\mathcal{A}_0^R\mathcal{A}_\perp^{R*})$	$\sin 2\theta_{K^*}\sin 2\theta_\ell\sin\phi$
9	$\beta_\ell^2\mathrm{Im}(\mathcal{A}_\parallel^{L*}\mathcal{A}_\perp^L+\mathcal{A}_\parallel^{R*}\mathcal{A}_\perp^R)$	$\sin^2\theta_{K^*}\sin^2\theta_\ell\sin 2\phi$

$$\mathcal{A}_0^{\mathrm{L,R}} = \frac{N_\ell\sqrt{N_{K^*}}}{2m_{K^*}\sqrt{q^2}}\left\{(C_9^{\mathrm{eff}} \mp C_{10})\left[(m_{B_s}^2 - m_{K^*}^2 - q^2)(m_{B_s}+m_{K^*})A_1(q^2) - \frac{\lambda}{m_{B_s}+m_{K^*}}A_2(q^2)\right]\right.$$
$$\left. + 2m_b C_7^{\mathrm{eff}}\left[(m_{B_s}^2 + 3m_{K^*}^2 - q^2)T_2(q^2) - \frac{\lambda}{m_{B_s}^2 - m_{K^*}^2}T_3(q^2)\right]\right\}, \tag{69}$$

$$\mathcal{A}_t = 2N_\ell\sqrt{N_{K^*}}\frac{\sqrt{\lambda}}{\sqrt{q^2}}C_{10}A_0(q^2), \tag{70}$$

where the factors N_ℓ and N_{K^*} are of the following form:

$$N_\ell = \frac{i\alpha_{em}G_F}{4\sqrt{2}\pi}V_{tb}V_{td}^*, \qquad N_{K^*} = \frac{8\beta_\ell\sqrt{\lambda}q^2}{3\times 256\pi^3 m_{B_s}^3}, \tag{71}$$

with $\lambda \equiv (m_{B_s}^2 - m_{K^*}^2 - q^2)^2 - 4m_{K^*}^2q^2$, $\beta_\ell = \sqrt{1-4m_\ell^2/q^2}$, and $\hat{m}_b = m_b/q^2$.

Analogous to Ref. [69], one can write down three partially integrated decay distributions, integrating all but one angle at a time. For the CP-conjugated process, we can do the similar operation using the corresponding decay distributions.

(1) The θ_{K^*} distribution:

$$\frac{d^2\Gamma}{dq^2 d\cos\theta_{K^*}} = a_{\theta_{K^*}}(q^2) + c_{\theta_{K^*}}(q^2)\cos^2\theta_{K^*},$$
$$a_{\theta_{K^*}}(q^2) = \frac{3}{8}(3I_1^s - I_2^s),$$
$$c_{\theta_{K^*}}(q^2) = \frac{3}{8}(3I_1^c - 3I_1^s - I_2^c + I_2^s). \tag{72}$$

(2) The θ_ℓ distribution:

$$\frac{d^2\Gamma}{dq^2 d\cos\theta_\ell} = a_{\theta_\ell}(q^2) + b_{\theta_\ell}(q^2)\cos\theta_\ell + c_{\theta_\ell}(q^2)\cos^2\theta_\ell,$$
$$a_{\theta_\ell}(q^2) = \frac{3}{8}(I_1^c + 2I_1^s - I_2^c - 2I_2^s),$$
$$b_{\theta_\ell}(q^2) = \frac{3}{4}(I_6^s),$$
$$c_{\theta_\ell}(q^2) = \frac{3}{4}(I_2^c + 2I_2^s). \tag{73}$$

(3) The ϕ distribution:

$$\frac{d^2\Gamma}{dq^2 d\phi} = a_\phi(q^2) + c_\phi^c(q^2)\cos 2\phi + c_\phi^s(q^2)\sin 2\phi,$$
$$a_\phi(q^2) = \frac{1}{8\pi}(3I_1^c + 6I_1^s - I_2^c - 2I_2^s),$$
$$c_\phi^c(q^2) = \frac{1}{2\pi}I_3,$$
$$c_\phi^s(q^2) = \frac{1}{2\pi}I_9. \tag{74}$$

From the full angular distributions as defined in Eq. (64), we set various coefficients apart and combine them into diverse quantities normalized to the differential decay rate and other observables [69]. Analogous observables are constructed for the CP-conjugated mode, after making the replacements as shown in Eq. (65) and (66).

(1) The differential decay rate:

$$\frac{d\Gamma}{dq^2} = \frac{1}{4}(3I_1^c + 6I_1^s - I_2^c - 2I_2^s), \tag{75}$$

(2) The lepton forward-backward asymmetry:

$$\mathcal{A}_{\mathrm{FB}}(q^2) = \frac{b_{\theta_\ell}(q^2)}{d\Gamma/dq^2} = \frac{3I_6^s}{3I_1^c + 6I_1^s - I_2^c - 2I_2^s}, \tag{76}$$

(3) The K^* polarization fraction:

$$R_{L,T}(q^2) = \frac{d\Gamma_L/dq^2}{d\Gamma_T/dq^2}, \tag{77}$$

where Γ_L and Γ_T represent the longitudinal and transverse K^* polarization decay rates,

$$\frac{d\Gamma_L}{dq^2} = \frac{2}{3}[a_{\theta_{K^*}}(q^2) + c_{\theta_{K^*}}(q^2)] = \frac{1}{4}(3I_1^c - I_2^c), \tag{78}$$

$$\frac{d\Gamma_T}{dq^2} = \frac{4}{3}a_{\theta_{K^*}}(q^2) = \frac{1}{2}(3I_1^s - I_2^s). \tag{79}$$

Alternatively, one can define the quantity $F_L^{K^*}$ which is a measure of the longitudinally polarized K^*'s in the whole ensemble of $B_s \to K^*\ell\ell$ decays, which is linked to $R_{L,T}(q^2)$ as

$$F_L^{K^*}(q^2) = \frac{R_{L,T}(q^2)}{1+R_{L,T}(q^2)} = \frac{1}{4}\cdot\frac{3I_1^c - I_2^c}{d\Gamma/dq^2} = \frac{3I_1^c - I_2^c}{3I_1^c + 6I_1^s - I_2^c - 2I_2^s}, \tag{80}$$

where $F_L^{K^*}$ is a number obtained by integrating $F_L^{K^*}(q^2)$ over the proper phase space.

(4) The direct CP asymmetry can also be defined in the same way as for $B_s \to Kl^+l^-$ decays:

$$\mathcal{A}_{CP}(q^2) = \frac{d\Gamma(\bar{B}_s \to K^* l^+ l^-)/dq^2 - d\bar{\Gamma}(B_s \to \bar{K}^* l^+ l^-)/dq^2}{d\Gamma(\bar{B}_s \to K^* l^+ l^-)/dq^2 + d\bar{\Gamma}(B_s \to \bar{K}^* l^+ l^-)/dq^2}. \tag{81}$$

The above observables are constructed from Eqs. (63) and (64) by integrating over the angles in various ranges. These observables which have a form factor dependence in the leading order are called *form factor dependent* observables and generally plagued by the large uncertainties of the form factors. To avoid this problem, a lot of work has been done to construct observables which are theoretically clean in the low-q^2 region. Such observables are free from this dependence at the leading order and are called *form factor independent* (FFI) observables. In this paper, we study both kinds of observables.

As a necessary and sufficient condition, such FFI observable must be invariant under the symmetry transformations of the transverse amplitudes A's; we then say that the observable respects the symmetries of the angular distribution. Fortunately, there exists a systematic procedure to construct all such possible observables as discussed in Ref. [68].

We start defining the following complex vectors [70]:

$$n_\parallel = \begin{pmatrix} A_\parallel^L \\ A_\parallel^{R*} \end{pmatrix}, \quad n_\perp = \begin{pmatrix} A_\perp^L \\ -A_\perp^{R*} \end{pmatrix}, \quad n_0 = \begin{pmatrix} A_0^L \\ A_0^{R*} \end{pmatrix}. \tag{82}$$

With these vectors we can construct the products $|n_i|^2 = n_i^\dagger n_i$ and $n_i^\dagger n_j$,

$$|n_\parallel|^2 = |A_\parallel^L|^2 + |A_\parallel^R|^2 = \frac{2I_2^s - I_3}{\beta_\ell^2}, \qquad n_\perp^\dagger n_\parallel = A_\perp^{L*}A_\parallel^L - A_\perp^R A_\parallel^{R*} = \frac{\beta_\ell I_6^s - 2iI_9}{2\beta_\ell^2}, \tag{83}$$

$$|n_\perp|^2 = |A_\perp^L|^2 + |A_\perp^R|^2 = \frac{2I_2^s + I_3}{\beta_\ell^2}, \qquad n_0^\dagger n_\parallel = A_0^{L*}A_\parallel^L + A_0^R A_\parallel^{R*} = \frac{2I_4 - i\beta_\ell I_7}{\sqrt{2}\beta_\ell^2}, \tag{84}$$

$$|n_0|^2 = |A_0^L|^2 + |A_0^R|^2 = -\frac{I_2^c}{\beta_\ell^2}, \qquad n_0^\dagger n_\perp = A_0^{L*}A_\perp^L - A_0^R A_\perp^{R*} = \frac{\beta_\ell I_5 - 2iI_8}{\sqrt{2}\beta_\ell^2}. \tag{85}$$

We examine the following (clean) FFI observables [68]:

$$P_1 = \frac{|n_\perp|^2 - |n_\parallel|^2}{|n_\perp|^2 + |n_\parallel|^2} = \frac{I_3}{2I_2^s}, \qquad P_2 = \frac{\mathrm{Re}(n_\perp^\dagger n_\parallel)}{|n_\parallel|^2 + |n_\perp|^2} = \beta_\ell \frac{I_6^s}{8I_2^s}, \tag{86}$$

$$P_3 = \frac{\mathrm{Im}(n_\perp^\dagger n_\parallel)}{|n_\parallel|^2 + |n_\perp|^2} = -\frac{I_9}{4I_2^s}, \qquad P_4 = \frac{\mathrm{Re}(n_0^\dagger n_\parallel)}{\sqrt{|n_\parallel|^2|n_0|^2}} = \frac{\sqrt{2}I_4}{\sqrt{-I_2^c(2I_2^s - I_3)}}, \tag{87}$$

$$P_5 = \frac{\mathrm{Re}(n_0^\dagger n_\perp)}{\sqrt{|n_\perp|^2|n_0|^2}} = \frac{\beta_\ell I_5}{\sqrt{-2I_2^c(2I_2^s + I_3)}}, \tag{88}$$

$$P_6 = \frac{\mathrm{Im}(n_0^\dagger n_\parallel)}{\sqrt{|n_\parallel|^2|n_0|^2}} = -\frac{\beta_\ell I_7}{\sqrt{-2I_2^c(2I_2^s - I_3)}}, \tag{89}$$

$$P_8 = \frac{\mathrm{Im}(n_0^\dagger n_\perp)}{\sqrt{|n_\perp|^2|n_0|^2}} = -\frac{\sqrt{2}I_8}{\sqrt{-I_2^c(2I_2^s + I_3)}}. \tag{90}$$

The primed observables are also defined in the following form [29]:

$$P_4' \equiv P_4\sqrt{1 - P_1} = \frac{I_4}{\sqrt{-I_2^c I_2^s}}, \qquad P_5' \equiv P_5\sqrt{1 + P_1} = \frac{\beta_\ell I_5}{2\sqrt{-I_2^c I_2^s}}, \tag{91}$$

$$P_6' \equiv P_6\sqrt{1 - P_1} = -\frac{\beta_\ell I_7}{2\sqrt{-I_2^c I_2^s}}, \qquad P_8' \equiv P_8\sqrt{1 + P_1} = -\frac{I_8}{\sqrt{-I_2^c I_2^s}}. \tag{92}$$

These primed observables $P'_{4,5,6,8}$ are clean and good approximations to $P_{4,5,6,8}$ due to the fact that $P_1 \simeq 0$ in the SM. From the experimental perspective, fitting the primed observables will be simpler and more efficient despite the fact that the whole analysis can be performed directly in terms of the observables $P_{4,5,6,8}$.

Since most observables are written in terms of the ratios, $O_i^\ell(q^2) = \mathcal{N}_i^\ell(q^2)/\mathcal{D}_i^\ell(q^2)$ with $\mathcal{N}$ and $\mathcal{D}$ being generically a numerator and a denominator, the integrated quantities are defined as in Ref. [69]:

$$\langle O_i^\ell \rangle = \frac{\int_{4m_\ell^2}^{q^2_{\rm max}} \mathcal{N}_i^\ell(q^2) dq^2}{\int_{4m_\ell^2}^{q^2_{\rm max}} \mathcal{D}_i^\ell(q^2) dq^2}. \tag{93}$$

We also check the physical observables $R^{e\mu}_{K,K^*}$ and $R^{\mu\tau}_{K,K^*}$, as defined in Eqs. (3) and (4), since the theoretical uncertainties are largely canceled in the ratio of the branching ratios of $B_s \to K^{(*)}\ell^+\ell^-$ decays.

In the region $q^2 < 4m_\mu^2$, where only the e^+e^- modes are allowed, there is a large enhancement of $B_s \to K^* e^+ e^-$ due to the $1/q^2$ scaling of the photon penguin contribution [71]. In order to remove the phase space effects in the ratio $R^{e\mu}_{K^*}$ and keep consistent with the other analysis [72], here we also use the lower cut of $4m_\mu^2$ for both the electron and muon modes in the definition of the ratio $R^{e\mu}_{K^*}$ as in Ref. [72]:

$$R^{e\mu}_{K^*} = \frac{\int_{4m_\mu^2}^{q^2_{\rm max}} dq^2 \frac{d\mathcal{B}(B_s \to K^* \mu^+\mu^-)}{dq^2}}{\int_{4m_\mu^2}^{q^2_{\rm max}} dq^2 \frac{d\mathcal{B}(B_s \to K^* e^+ e^-)}{dq^2}}. \tag{94}$$

V. NUMERICAL RESULTS AND DISCUSSIONS

In the numerical calculations we use the following input parameters (here masses and decay constants are in units of GeV) [30,31]:

$$\begin{aligned} &\Lambda^{f=4}_{\overline{\rm MS}} = 0.250, \quad \tau_{B_s^0} = 1.509 ps, \quad m_b = 4.8, \quad m_W = 80.38, \\ &m_K = 0.498, \quad m_{K^*} = 0.892, \quad m_{B_s} = 5.367, \quad m_\tau = 1.777, \\ &f_{B_s} = 0.23, \quad f_K = 0.16, \quad f_{K^*} = 0.217, \quad f^T_{K^*} = 0.185, \end{aligned} \tag{95}$$

For the CKM matrix elements and angles, we use the values as given in PDG 2018 [30]:

$$\begin{aligned} &V_{tb} = 1.019 \pm 0.025, \quad V_{ud} = 0.97420 \pm 0.00021, \\ &V_{td} = |V_{td}| \cdot e^{-i\beta}, \quad |V_{td}| = (8.1 \pm 0.5) \times 10^{-3}, \quad \sin(2\beta) = 0.691 \pm 0.017, \\ &V_{ub} = |V_{ub}| \cdot e^{-i\gamma}, \quad |V_{ub}| = (3.94 \pm 0.36) \times 10^{-3}, \quad \gamma = (73.5^{+4.2}_{-5.1})^\circ. \end{aligned} \tag{96}$$

A. The form factors

For the considered semileptonic decays, the differential decay rates and other physical observables strongly rely on the value and the shape of the relevant form factors $F_{0,+}(q^2)$ and $F_T(q^2)$ for $B_s \to K\ell^+\ell^-$ decays, and the form factors $V(q^2)$, $A_{0,1,2}(q^2)$ and $T_{1,2,3}(q^2)$ for $B_s \to K^*\ell^+\ell^-$ decays. These form factors have been calculated in rather different theories or models, such as the relativistic quark model (RQM) [73], the LCSR [28,74], and the covariant confined quark model (CCQM) [75]. For the heavy B/B_s to light meson (such as K, π, η', ρ, K^*, etc.) transitions, on the other hand, the relevant form factors at the low-q^2 region have been evaluated successfully by employing the PQCD factorization approach, for example, in Refs. [26,27,33–35,41,42,76].

Since the PQCD predictions for the considered form factors are reliable only at the low-q^2 region, we usually calculate explicitly the values of the relevant form factors at the low-q^2 region, say $0 \le q^2 \le m_\tau^2$, and then make an extrapolation for all relevant form factors from the low-q^2 region to the large-q^2 region by using the pole model parametrization [77,78] or other different methods.

In Refs. [79–81], we developed a new method: the so-called PQCD + Lattice approach. Here we still use the PQCD approach to evaluate the form factors at the low-q^2 region, but take those currently available lattice QCD results for the relevant form factors at the high-q^2 region as the lattice QCD input to improve the extrapolation of the form factors up to $q^2_{\rm max}$. In Refs. [80,81], we used the BCL parametrization method [36,37] instead of the traditional pole model parametrization since the BCL method has better convergence.

In Tables IV and V, we list the values of the lattice QCD results for the relevant $B_s \to K^*$ transition form factors at

TABLE IV. The values for the lattice QCD results of the relevant $B_s \to K$ transition form factors at three reference points of q^2: $q^2 = 17.9, 21.2$ GeV^2 and $q^2_{\rm max} = (m_{B_s} - m_K)^2 \approx 23.8$ GeV^2 [82].

	q^2 Point		
FF	17.9	21.2	23.8
$F_0(q^2)$	0.48(5)	0.63(5)	0.80(5)
$F_+(q^2)$	0.98(7)	1.64(10)	2.76(16)

TABLE V. The values for the lattice QCD results of the relevant $B_s \to K^*$ transition form factors at three reference points of q^2: $q^2 = 12$, 16 GeV^2 and $q^2_{\rm max} = (m_{B_s} - m_{K^*})^2 \approx 20$ GeV^2 [83].

q^2	$V(q^2)$	$A_0(q^2)$	$A_1(q^2)$	$A_2(q^2)$	$T_1(q^2)$	$T_2(q^2)$	$T_3(q^2)$
12	0.56(9)	0.84(9)	0.37(3)	0.46(3)	0.61(4)	0.39(3)	0.43(4)
16	1.02(8)	1.33(8)	0.45(3)	0.60(5)	0.90(6)	0.47(3)	0.67(5)
20	1.99(13)	2.38(16)	0.58(3)	0.85(12)	1.48(10)	0.60(3)	1.10(7)

three reference points of q^2 [82,83] used in this paper. The systematic uncertainties are included.

In this work, we will use both the PQCD factorization approach and the PQCD + Lattice approach to evaluate all relevant form factors over the whole range of q^2.

(1) In the PQCD approach, we use the definitions and formulas as given in Eqs. (38)–(42), and (44)–(50) to calculate the values of all relevant form factors $F_{0,+,T}(q^2)$, $V(q^2)$, $A_{0,1,2}(q^2)$, and $T_{1,2,3}(q^2)$ in the low-q^2 region: $0 \le q^2 \le m_\tau^2$. We then make the extrapolation for these form factors to the large-q^2 region up to $q^2_{\rm max}$ by using the proper parametrization method.

(2) In the PQCD + Lattice approach, we take the lattice QCD results for the form factors at some large-q^2 points as inputs and then make a combined fit to the PQCD and the lattice QCD results at the low- and high q^2-region.

(3) For both approaches, we always use the same z-series parametrization as in Refs. [29,74] to make the extrapolation:

$$z(q^2) = \frac{\sqrt{t_+ - q^2} - \sqrt{t_+ - t_0}}{\sqrt{t_+ - q^2} + \sqrt{t_+ - t_0}} \qquad (97)$$

where $t_\pm = (m_{B_s} \pm m_{K^{(*)}})^2$ and $t_0 = t_+(1 - \sqrt{1 - t_-/t_+})$. Form factors are parametrized as

$$F_i(q^2) = P_i(q^2)\Sigma_k \alpha_k^i [z(q^2) - z(0)]^k, \qquad (98)$$

where $P_i(q^2) = (1 - q^2/m^2_{R,i})^{-1}$ is a simple pole corresponding to the $\bar{d}b$ resonance with appropriate J^P in the spectrum and $m_{R,i}$ is the resonance mass: $m_R \to \infty$ for $F_0(q^2)$ (no pole), 5.279 GeV for $A_0(q^2)$ couple to $B(0^-)$, 5.325 GeV for $F_{+,T}(q^2)$, $V(q^2)$ and $T_1(q^2)$ couple to $B^*(1^-)$, and 5.724 GeV for the rest of the form factors couple to $B_1(1^+)$.

In Table VI, as a comparison, we show the center values of all relevant form factors in this work and other theoretical predictions as given in Refs. [26,28,44,73,84–89] at the scale $q^2 = 0$. The PQCD factorization approach is applied in Refs. [44,86] and in Ref. [26] with the inclusion of the NLO corrections. The CCQM is used in Ref. [75]. Calculations are based on LCSRs in Refs. [28,74] with hadronic input parameters and in Ref. [84] with the inclusion of the one-loop radiative corrections. In Ref. [73], the authors used the relativistic quark model based on the quasipotential approach. In Ref. [85], the authors used the quark model and relativistic dispersion approach. In Ref. [87], the light-cone quark model is utilized based on the basis of the soft collinear effective theory. The authors of Ref. [88] employed the LCSR in the framework of the heavy quark effective theory. In Ref. [89], the authors evaluated the transition form factors in the six-quark effective Hamiltonian approach. One can see that there is no significant difference between the theoretical predictions for the $B_s \to K^{(*)}$ transition form factors evaluated at $q^2 = 0$ in various models or approaches.

In Table VII, we list the PQCD predictions for the form factors $F_{+,0,T}(q^2)$, $V(q^2)$, $A_{0,1,2}(q^2)$, and $T_{1,2,3}(q^2)$ with the corresponding pole and resonance masses, and the fitting parametrization constants $(\alpha_0, \alpha_1, \alpha_2)$ in Eq. (98) for $B_s \to K^{(*)}$ transitions. It is simple to figure out the relation $F_i(0) = \alpha_0^i$ by substituting q^2 with zero on both sides of Eq. (98). The theoretical errors of the form factors as

TABLE VI. The theoretical predictions for the center values of the form factors of the $B_s \to K^{(*)}$ transitions at $q^2 = 0$ obtained by using rather different theories or models.

	$F_{0,+}(0)$	$F_T(0)$	$V(0)$	$A_0(0)$	$A_1(0)$	$A_2(0)$	$T_{1,2}(0)$	$T_3(0)$
This paper	0.22	0.22	0.24	0.21	0.19	0.19	0.21	0.16
PQCD[26]	0.26	0.28	⋯	⋯	⋯	⋯	⋯	⋯
PQCD[86]	⋯	⋯	0.20	0.24	0.15	0.11	0.18	0.16
PQCD[44]	0.24	⋯	0.21	0.25	0.16	⋯	⋯	⋯
CCQM[75]	⋯	⋯	0.24	0.18	0.21	0.21	0.21	0.14
LCSR[28]	0.336	0.320	⋯	⋯	⋯	⋯	⋯	⋯
LCSR[74]	⋯	⋯	0.296	0.314	0.230	⋯	0.239	⋯
LCSR[84]	0.30	⋯	0.311	0.360	0.233	0.181	0.260	0.136
RQM[73]	0.284	0.236	0.291	0.289	0.287	0.286	0.238	0.122
RDA[85]	0.31	0.31	0.38	0.37	0.29	0.26	0.32	0.23
SCET[87]	0.290	0.317	0.323	0.279	0.232	0.210	0.271	0.165
HQEFT[88]	0.296	0.288	0.285	0.222	0.227	0.183	0.251	0.169
SQEH[89]	0.260	⋯	0.227	0.280	0.178	⋯	⋯	⋯

TABLE VII. The PQCD predictions for the form factors of $B_s \to K^{(*)}$ transitions. Form factors $F_{+,0,T}(q^2)$, $V(q^2)$, $A_{0,1,2}(q^2)$, and $T_{1,2,3}(q^2)$ are fitted by using Eq. (98).

PQCD	$B(J^P)$	α_0	α_1	α_2
$F_+^{B_s\to K}$	$B^*(1^-)$	$0.22^{+0.04}_{-0.06}(\omega_{B_s}) \pm 0.005(a_i^K)$	$-1.21^{+0.36}_{-0.23} \pm 0.02$	$0.06^{+1.74}_{-1.09} \pm 0.14$
$F_0^{B_s\to K}$	no pole	$0.22^{+0.04}_{-0.06}(\omega_{B_s}) \pm 0.005(a_i^K)$	$-1.31^{+0.40}_{-0.24} \pm 0.03$	$-0.22^{+1.73}_{-1.11} \pm 0.13$
$F_T^{B_s\to K}$	$B^*(1^-)$	$0.22^{+0.04}_{-0.06}(\omega_{B_s}) \pm 0.005(a_i^K)$	$-1.37^{+0.40}_{-0.29} \pm 0.03$	$7.05^{+1.85}_{-1.08} \pm 0.15$
$V^{B_s\to K^*}$	$B^*(1^-)$	$0.24^{+0.05}_{-0.04}(\omega_{B_s}) \pm 0.005(a_i^{K^*})$	$-1.87^{+0.31}_{-0.42} \pm 0.03$	$7.56^{+1.22}_{-1.41} \pm 0.13$
$A_0^{B_s\to K^*}$	$B^0(0^-)$	$0.21^{+0.04}_{-0.03}(\omega_{B_s}) \pm 0.003(a_i^{K^*})$	$-1.43^{+0.25}_{-0.29} \pm 0.02$	$8.28^{+1.38}_{-1.03} \pm 0.11$
$A_1^{B_s\to K^*}$	$B_1(1^+)$	$0.19^{+0.04}_{-0.03}(\omega_{B_s}) \pm 0.003(a_i^{K^*})$	$-0.64^{+0.13}_{-0.14} \pm 0.01$	$0.35^{+1.04}_{-1.02} \pm 0.10$
$A_2^{B_s\to K^*}$	$B_1(1^+)$	$0.19^{+0.04}_{-0.03}(\omega_{B_s}) \pm 0.003(a_i^{K^*})$	$-1.42^{+0.28}_{-0.31} \pm 0.03$	$2.77^{+1.68}_{-1.07} \pm 0.12$
$T_1^{B_s\to K^*}$	$B^*(1^-)$	$0.21^{+0.04}_{-0.03}(\omega_{B_s}) \pm 0.003(a_i^{K^*})$	$-1.52^{+0.24}_{-0.34} \pm 0.03$	$9.10^{+1.35}_{-1.46} \pm 0.13$
$T_2^{B_s\to K^*}$	$B_1(1^+)$	$0.21^{+0.04}_{-0.03}(\omega_{B_s}) \pm 0.003(a_i^{K^*})$	$-0.44^{+0.13}_{-0.08} \pm 0.01$	$4.38^{+1.33}_{-1.93} \pm 0.16$
$T_3^{B_s\to K^*}$	$B_1(1^+)$	$0.16^{+0.03}_{-0.02}(\omega_{B_s}) \pm 0.002(a_i^{K^*})$	$-0.99^{+0.19}_{-0.27} \pm 0.02$	$8.12^{+1.04}_{-1.81} \pm 0.11$

shown in Table VII are the two major errors from the uncertainties of the parameter $\omega_{B_s} = 0.50 \pm 0.05$ GeV and the Gegenbauer moments in the distribution amplitudes $a_i^K(a_i^{K^*})$ of the light pseudoscalar (vector) mesons. The additional theoretical uncertainties from other input parameters, such as the decay constants $f_{B_s}, f_K, f_{K^*}, f_{K^*}^T$, are very small and have been neglected.

In Table VIII, we list the PQCD + Lattice predictions for the form factors $F_{+,0}(q^2)$, $V(q^2)$, $A_{0,1,2}(q^2)$, and $T_{1,2,3}(q^2)$ by taking into account the lattice QCD results for the form factors at some points of q^2 as listed in Tables IV and V from Refs. [82,83], in a similar way as what we did in Refs. [79–81]. The errors are obtained in the same way as those in Table VII. The additional form factors $A_{12}(q^2)$ and $T_{23}(q^2)$ can be defined as the linear combinations of $A_1(q^2)$ and $A_2(q^2)$, $T_2(q^2)$ and $T_3(q^2)$, together the with kinematic variable λ as given in Eqs. (10) and (11) from Ref. [83]. In Figs. 3 and 4, we show the q^2 dependence of the form factors $F_{+,0,T}(q^2)$, $V(q^2)$, $A_{0,1,2}(q^2)$, and $T_{1,2,3}(q^2)$ in the PQCD (the red curves) and PQCD + Lattice (the blue curves) approaches for $B_s \to K^{(*)}$ transitions. The error bars of the initial PQCD and relevant lattice QCD results as listed in Tables IV and V are blackened, in order to show them clearly.

B. Observables for $B_s \to K\ell^+\ell^-$

From the differential decay rates as given in Eq. (58), it is conventional to make the integration over the range of $4m_\ell^2 \le q^2 \le (m_{B_s} - m_K)^2$. In order to be consistent with the choices made by experiment collaborations in their data analysis, however, we have to cut off the regions of the dilepton mass squared around the charmonium resonances $J/\psi(1S)$ and $\psi(2S)$: i.e., $8.0 < q^2 < 11.0$ GeV^2 and $12.5 < q^2 < 15.0$ GeV^2 for $\ell = (e, \mu, \tau)$ cases. The PQCD and PQCD + Lattice predictions for the BRs and the longitudinal polarization asymmetry P_L of the semileptonic decays $\bar{B}_s \to K\ell^+\ell^-$ and $B_s \to \bar{K}\ell^+\ell^-$ at three different renormalization scales $\mu = (0.5m_b, m_b, 1.5m_b)$ are listed in Tables IX and X, respectively, where the total theoretical errors are the combinations of the uncertainties of all relevant input parameters: ω_{B_s}, a_i^K and V_{ij}. The direct CP asymmetries $\mathcal{A}_{CP}$ are obtained by making integration

TABLE VIII. The PQCD + Lattice predictions for the form factors of $B_s \to K^{(*)}$ transitions. All form factors are fitted by using Eq. (98).

PQCD + Lattice	$B(J^P)$	α_0	α_1	α_2
$F_+^{B_s\to K}$	$B^*(1^-)$	$0.22^{+0.04}_{-0.06}(\omega_{B_s}) \pm 0.005(a_i^K)$	$-0.89^{+0.23}_{-0.36} \pm 0.02$	$-0.44^{+0.37}_{-0.44} \pm 0.03$
$F_0^{B_s\to K}$	No pole	$0.22^{+0.04}_{-0.06}(\omega_{B_s}) \pm 0.005(a_i^K)$	$-0.50^{+0.08}_{-0.15} \pm 0.01$	$5.07^{+0.27}_{-0.31} \pm 0.02$
$V^{B_s\to K^*}$	$B^*(1^-)$	$0.24^{+0.05}_{-0.03}(\omega_{B_s}) \pm 0.005(a_i^{K^*})$	$-0.13^{+0.11}_{-0.07} \pm 0.01$	$10.14^{+0.47}_{-0.49} \pm 0.04$
$A_0^{B_s\to K^*}$	$B^0(0^-)$	$0.21^{+0.03}_{-0.03}(\omega_{B_s}) \pm 0.003(a_i^{K^*})$	$-3.38^{+0.17}_{-0.15} \pm 0.02$	$-4.13^{+0.43}_{-0.49} \pm 0.04$
$A_1^{B_s\to K^*}$	$B_1(1^+)$	$0.19^{+0.04}_{-0.03}(\omega_{B_s}) \pm 0.004(a_i^{K^*})$	$-0.65^{+0.27}_{-0.15} \pm 0.02$	$-2.66^{+0.43}_{-0.32} \pm 0.03$
$A_2^{B_s\to K^*}$	$B_1(1^+)$	$0.19^{+0.04}_{-0.03}(\omega_{B_s}) \pm 0.004(a_i^{K^*})$	$-1.35^{+0.58}_{-0.55} \pm 0.04$	$-3.12^{+1.96}_{-1.43} \pm 0.15$
$T_1^{B_s\to K^*}$	$B^*(1^-)$	$0.21^{+0.04}_{-0.03}(\omega_{B_s}) \pm 0.003(a_i^{K^*})$	$-1.85^{+0.30}_{-0.19} \pm 0.02$	$-3.23^{+1.26}_{-1.32} \pm 0.12$
$T_2^{B_s\to K^*}$	$B_1(1^+)$	$0.21^{+0.04}_{-0.03}(\omega_{B_s}) \pm 0.003(a_i^{K^*})$	$-0.65^{+0.29}_{-0.16} \pm 0.02$	$-2.85^{+0.73}_{-0.55} \pm 0.05$
$T_3^{B_s\to K^*}$	$B_1(1^+)$	$0.16^{+0.03}_{-0.02}(\omega_{B_s}) \pm 0.002(a_i^{K^*})$	$-1.00^{+0.19}_{-0.15} \pm 0.02$	$2.82^{+1.26}_{-1.08} \pm 0.09$

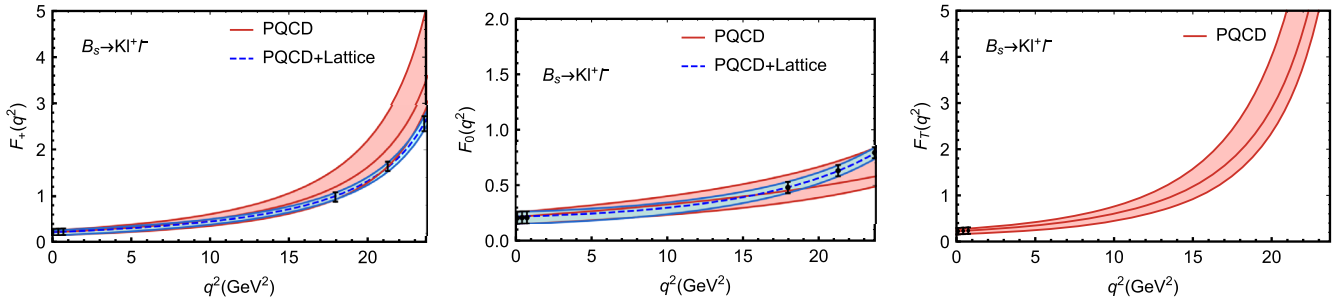

FIG. 3. The q^2 dependence of the form factors $F_{+,0,T}(q^2)$ in the PQCD (red) and PQCD + Lattice (blue) approaches for $B_s \to K$ transition, while the red (blue) shaded band shows the major theoretical uncertainty.

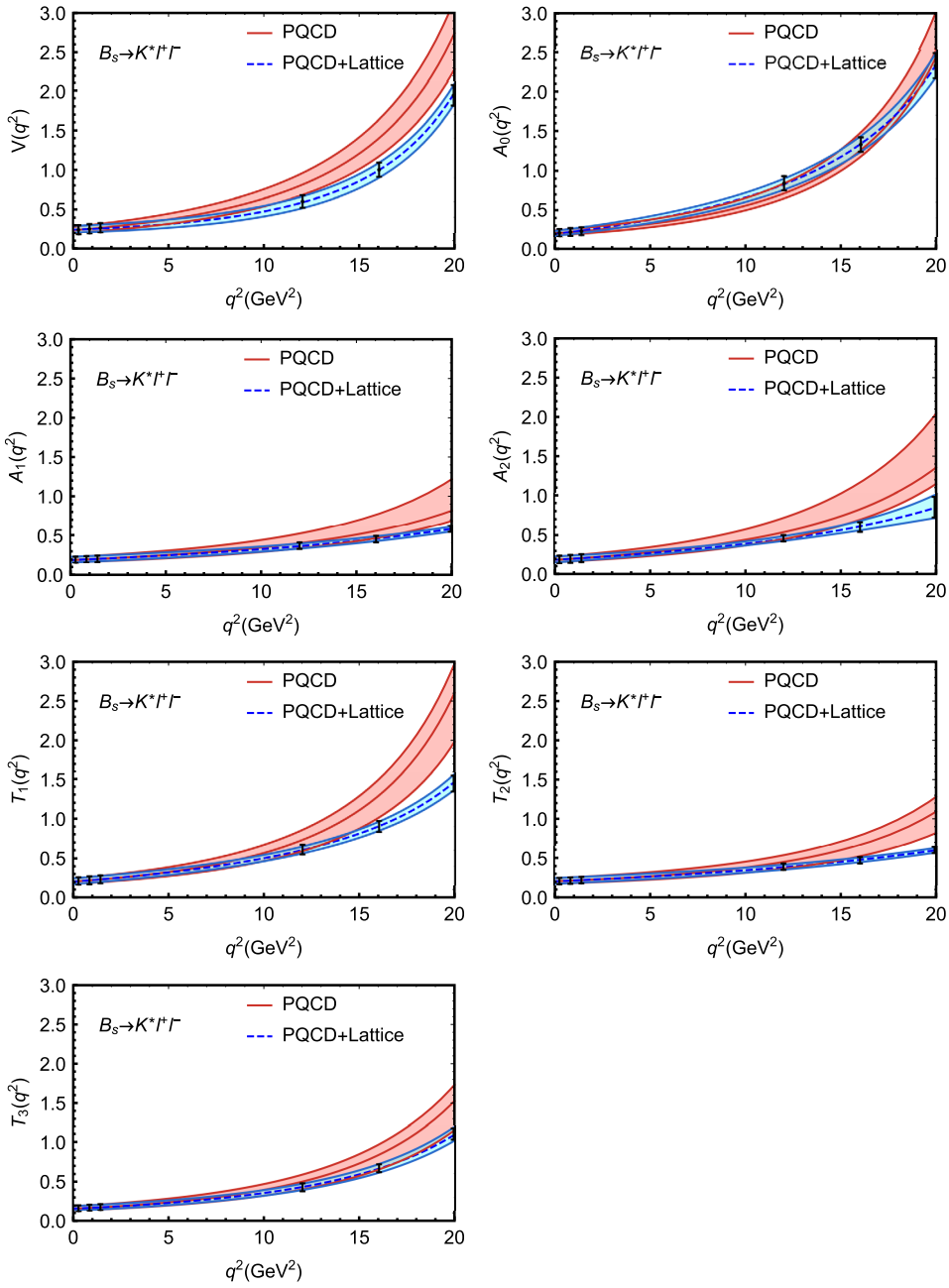

FIG. 4. The q^2 dependence of the form factors $V(q^2)$, $A_{0,1,2}(q^2)$, and $T_{1,2,3}(q^2)$ in the PQCD (red) and PQCD + Lattice (blue) approaches for $B_s \to K^*$ transition, while the red (blue) shaded band shows the major theoretical uncertainty.

TABLE IX. The PQCD predictions for the branching ratios (in units of 10^{-8}), the longitudinal polarization asymmetry P_L and the ratios $(R_K^{e\mu}, R_K^{\mu\tau})$ of the decays $\bar{B}_s \to K\ell^+\ell^-$ (the first row) and $B_s \to \bar{K}\ell^+\ell^-$ (the second row) at three different renormalization scales. The direct CP asymmetries $\mathcal{A}_{CP}$ (in units of 10^{-2}) are also listed.

Mode	Observables	$\mu = 0.5m_b$	$\mu = m_b$	$\mu = 1.5m_b$	PQCD[26]
$\ell = e$	$\mathcal{B}(\bar{B}_s \to K\ell^+\ell^-)$	$1.17^{+0.68}_{-0.56}$	$1.24^{+0.70}_{-0.60}$	$1.26^{+0.71}_{-0.61}$	$1.63^{+0.73}_{-0.58}$
	$\mathcal{B}(B_s \to \bar{K}\ell^+\ell^-)$	$1.21^{+0.68}_{-0.59}$	$1.32^{+0.73}_{-0.64}$	$1.63^{+0.74}_{-0.66}$	⋯
	$P_L(\bar{B}_s \to K\ell^+\ell^-)$	-0.986 ± 0.002	-0.979 ± 0.002	-0.972 ± 0.002	⋯
	$P_L(B_s \to \bar{K}\ell^+\ell^-)$	-0.980 ± 0.002	-0.954 ± 0.008	-0.937 ± 0.004	⋯
	$\mathcal{A}_{CP}$	-1.7 ± 0.9	-3.1 ± 0.4	-3.8 ± 0.6	⋯
$\ell = \mu$	$\mathcal{B}$	$1.17^{+0.68}_{-0.56}$	$1.24^{+0.71}_{-0.60}$	$1.25^{+0.71}_{-0.61}$	$1.63^{+0.73}_{-0.58}$
		$1.21^{+0.68}_{-0.69}$	$1.32^{+0.73}_{-0.64}$	$1.35^{+0.74}_{-0.66}$	⋯
	P_L	-0.974 ± 0.002	-0.966 ± 0.002	-0.959 ± 0.002	⋯
		-0.964 ± 0.003	-0.938 ± 0.005	-0.920 ± 0.004	⋯
	$\mathcal{A}_{CP}$	-1.7 ± 0.9	-3.1 ± 0.4	-3.8 ± 0.6	⋯
$\ell = \tau$	$\mathcal{B}$	$0.380^{+0.202}_{-0.157}$	$0.382^{+0.204}_{-0.158}$	$0.377^{+0.203}_{-0.156}$	$0.43^{+0.18}_{-0.15}$
		$0.382^{+0.202}_{-0.158}$	$0.386^{+0.206}_{-0.159}$	$0.382^{+0.204}_{-0.158}$	⋯
	P_L	-0.347 ± 0.002	-0.348 ± 0.002	-0.346 ± 0.002	⋯
		-0.348 ± 0.002	-0.349 ± 0.002	-0.348 ± 0.001	⋯
	$\mathcal{A}_{CP}$	-0.3 ± 0.2	-0.5 ± 0.2	-0.7 ± 0.2	⋯
	$R_K^{e\mu}$	0.996 ± 0.002	0.996 ± 0.002	0.996 ± 0.002	1
		0.996 ± 0.002	0.996 ± 0.002	0.996 ± 0.002	⋯
	$R_K^{\mu\tau}$	0.332 ± 0.045	0.325 ± 0.045	0.322 ± 0.045	0.26
		0.320 ± 0.046	0.303 ± 0.046	0.296 ± 0.046	⋯

over q^2 for $\mathcal{A}_{CP}(q^2)$ as defined in Eqs. (62) and (81) and are also listed in these two tables. To reduce the large theoretical uncertainties, we also check the physical observables $R_K^{e\mu}$ and $R_K^{\mu\tau}$, as defined in Eqs. (3) and (4), i.e., the ratio of the branching ratios of $B_s \to K\ell^+\ell^-$ decays. As a comparison, the previous PQCD predictions as given in Ref. [26] for the decay rates and the ratios $R_K^{e\mu}$ and $R_K^{\mu\tau}$ are listed in last column of Table s IX and X.

TABLE X. The PQCD + Lattice predictions for the branching ratios (in unit of 10^{-8}), the longitudinal polarization asymmetry P_L and the direct CP asymmetry $\mathcal{A}_{CP}$ (in unit of 10^{-2}), as well as the ratios $(R_K^{e\mu}, R_K^{\mu\tau})$ of the decays $\bar{B}_s \to K\ell^+\ell^-$ (the first row) and $B_s \to \bar{K}\ell^+\ell^-$ (the second row) at three different renormalization scales.

Mode	Observables	$\mu = 0.5m_b$	$\mu = m_b$	$\mu = 1.5m_b$	PQCD [26]
$\ell = e$	$\mathcal{B}(\bar{B}_s \to K\ell^+\ell^-)$	$0.95^{+0.26}_{-0.31}$	$1.01^{+0.29}_{-0.33}$	$1.03^{+0.28}_{-0.35}$	$1.63^{+0.73}_{-0.58}$
	$\mathcal{B}(B_s \to \bar{K}\ell^+\ell^-)$	$0.99^{+0.27}_{-0.33}$	$1.10^{+0.31}_{-0.38}$	$1.14^{+0.32}_{-0.40}$	⋯
	$P_L(\bar{B}_s \to K\ell^+\ell^-)$	-0.983 ± 0.007	-0.975 ± 0.005	-0.967 ± 0.006	⋯
	$P_L(B_s \to \bar{K}\ell^+\ell^-)$	-0.977 ± 0.008	-0.949 ± 0.013	-0.930 ± 0.010	⋯
	$\mathcal{A}_{CP}$	-2.0 ± 0.5	-4.3 ± 1.4	-5.0 ± 0.8	⋯
$\ell = \mu$	$\mathcal{B}$	$0.95^{+0.25}_{-0.31}$	$1.01^{+0.27}_{-0.33}$	$1.03^{+0.28}_{-0.34}$	$1.63^{+0.73}_{-0.58}$
		$0.99^{+0.27}_{-0.33}$	$1.10^{+0.31}_{-0.38}$	$1.13^{+0.32}_{-0.40}$	⋯
	P_L	-0.968 ± 0.008	-0.960 ± 0.007	-0.953 ± 0.008	⋯
		-0.958 ± 0.009	-0.929 ± 0.012	-0.911 ± 0.014	⋯
	$\mathcal{A}_{CP}$	-2.0 ± 0.5	-4.3 ± 1.4	-5.1 ± 0.8	⋯
$\ell = \tau$	$\mathcal{B}$	$0.365^{+0.072}_{-0.075}$	$0.368^{+0.072}_{-0.076}$	$0.365^{+0.072}_{-0.075}$	$0.43^{+0.18}_{-0.15}$
		$0.366^{+0.072}_{-0.075}$	$0.370^{+0.073}_{-0.076}$	$0.368^{+0.073}_{-0.076}$	⋯
	P_L	-0.234 ± 0.020	-0.235 ± 0.018	-0.233 ± 0.019	⋯
		-0.234 ± 0.020	-0.237 ± 0.019	-0.236 ± 0.019	⋯
	$\mathcal{A}_{CP}$	-0.1 ± 0.1	-0.3 ± 0.1	-0.4 ± 0.1	⋯
	$R_K^{e\mu}$	0.996 ± 0.002	0.996 ± 0.002	0.996 ± 0.002	1
		0.996 ± 0.002	0.996 ± 0.002	0.996 ± 0.002	⋯
	$R_K^{\mu\tau}$	0.395 ± 0.081	0.384 ± 0.080	0.381 ± 0.080	0.26
		0.375 ± 0.084	0.350 ± 0.085	0.341 ± 0.085	⋯

In order to show the major theoretical uncertainties from different sources explicitly, for instance, we show the PQCD predictions for $\mathcal{B}(\bar{B}_s \to K\mu^+\mu^-)$ with the four kinds of errors:

$$\mathcal{B}(\bar{B}_s \to K\mu^+\mu^-) = (1.24^{+0.69}_{-0.58}(\omega_{B_s}) \pm 0.15(a_i^K) \pm 0.06(V_{ij})^{+0.01}_{-0.07}(\mu)) \times 10^{-8}, \quad (99)$$

where the dominant theoretical error comes from $\omega_{B_s} = 0.50 \pm 0.05$, the second one from the Gegenbauer moments $a_1^K = 0.06 \pm 0.03$ and $a_2^K = 0.25 \pm 0.15$ as given in Eq. (17), the third one from the CKM elements V_{ij} in Eq. (96), and the last error from the renormalization scale $\mu = (1 \pm 0.5)m_b$. The possible errors from other input parameters are very small and have been neglected.

From Tables IX and X, it is easy to find the CP-averaged decay rates and the direct CP asymmetries $\mathcal{A}_{CP}$ for the considered semileptonic decays:

$$\mathcal{B}(\bar{B}_s \to Kl^+l^-)|_{\text{CP-av.}} = \begin{cases} (1.28^{+0.52}_{-0.48}) \times 10^{-8}, & \text{PQCD}, \\ (1.06^{+0.22}_{-0.29}) \times 10^{-8}, & \text{PQCD + Lattice}, \end{cases} \quad (100)$$

$$\mathcal{A}_{CP}(\bar{B}_s \to Kl^+l^-) = \begin{cases} -(3.1^{+0.8}_{-1.5}) \times 10^{-2}, & \text{PQCD}, \\ -(4.3^{+1.6}_{-2.7}) \times 10^{-2}, & \text{PQCD + Lattice}, \end{cases} \quad (101)$$

for the case of $l = (e, \mu)$, and

$$\mathcal{B}(\bar{B}_s \to K\tau^+\tau^-)|_{\text{CP-av.}} = \begin{cases} (0.38^{+0.14}_{-0.12}) \times 10^{-8}, & \text{PQCD}, \\ (0.37^{+0.05}_{-0.06}) \times 10^{-8}, & \text{PQCD + Lattice}, \end{cases} \quad (102)$$

$$\mathcal{A}_{CP}(\bar{B}_s \to K\tau^+\tau^-) = \begin{cases} -(0.5 \pm 0.3) \times 10^{-2}, & \text{PQCD}, \\ -(0.3 \pm 0.2) \times 10^{-2}, & \text{PQCD + Lattice}, \end{cases} \quad (103)$$

for the case of τ lepton.

In Fig. 5, we show the q^2 dependence of the theoretical predictions of the differential branching fraction $d\mathcal{B}/dq^2$ and the longitudinal lepton polarization $P_L(q^2)$ for the decays $\bar{B}_s \to K\ell^+\ell^-$ with $l = (\mu, \tau)$, evaluated by using the PQCD (the red solid curves) and the PQCD + Lattice (the blue dashed curves) approach, with the choice of the scale $\mu = m_b$ and $q^2_{\text{max}} = 23.71\ \text{GeV}^2$. The shaded bands indicate the theoretical error of our predictions due to the uncertainties of the input parameters. The two vertical grey blocks are the experimental veto regions [1] in order to remove contributions from $\bar{B}_s \to J/\psi(1S)(\to \ell^+\ell^-)K$ (the left-hand band) and $\bar{B}_s \to \psi'(2S)(\to \ell^+\ell^-)K$ (the right-hand band) for the q^2 dependence of $d\mathcal{B}/dq^2$ and P_L. The figure for the electron mode is almost identical with the one for muon, and therefore not shown here.

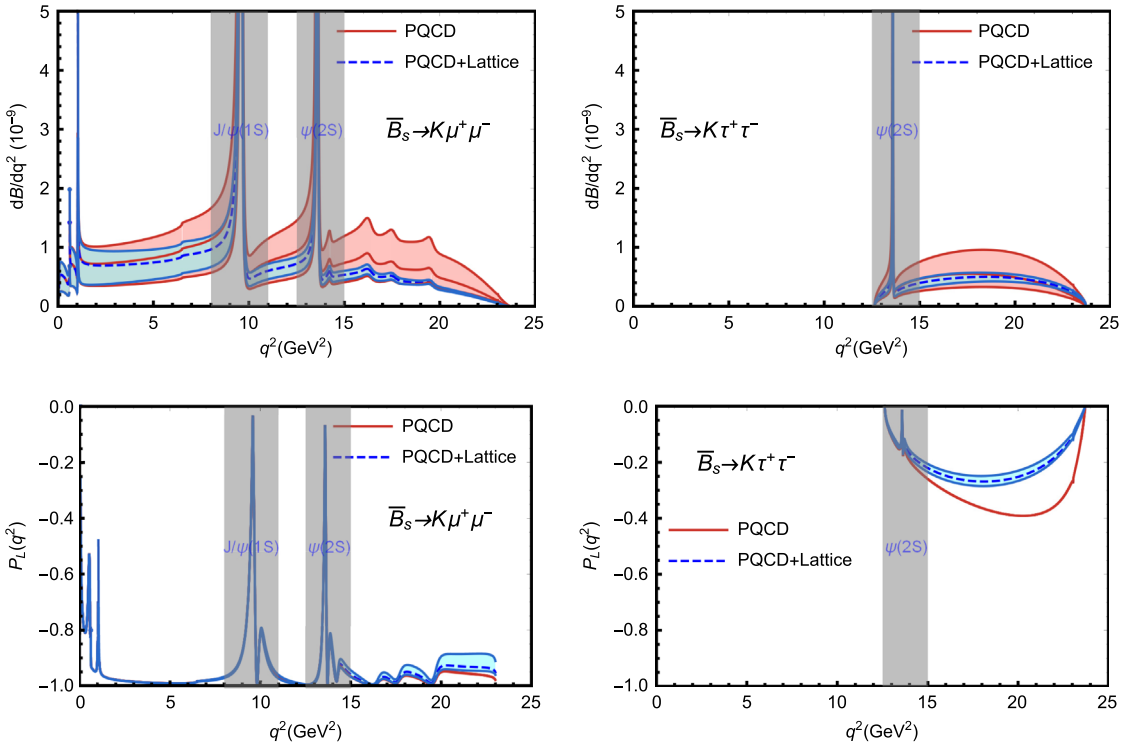

FIG. 5. The PQCD or "PQCD + Lattice" predictions for the q^2-dependence of $d\mathcal{B}/dq^2$ and $P_L(q^2)$ for the decays $\bar{B}_s \to K\ell^+\ell^-$ with $l = \mu, \tau$. For details see the text.

From the numerical results as listed in Tables IX and X, one can see the following points:

(1) The theoretical predictions from both PQCD and PQCD + Lattice approaches have a relatively weak dependence on the choice of the renormalization scale μ. The variations of the central values due to the μ dependence are about 10% in magnitude and smaller than the combined errors from the uncertainties of other input parameters.

(2) Because of the term proportional to λ_u in the effective Hamiltonian $\mathcal{H}_{\rm eff}$ in Eq. (25), the PQCD and PQCD + Lattice predictions for the considered observables for $\bar{B}_s \to K l^+ l^-$ and its CP conjugated mode have a relatively small differences, roughly (5–15)% in magnitude. For the CP-averaged branching ratios, the PQCD and PQCD + Lattice predictions agree well within 1 standard deviation. As generally expected, the direct CP asymmetries $\mathcal{A}_{CP}$ are very small: less than 5%.

(3) For the ratio $R_K^{e\mu}$, we find $R_K^{e\mu} = 0.996(2)$ in both the PQCD and PQCD + Lattice approaches. For the ratio $R_K^{\mu\tau}$, the PQCD prediction is about 0.33 and a little smaller than the PQCD + Lattice prediction $R_K^{\mu\tau} \approx 0.39$, and they also show a weak μ dependence: less than 9% in magnitude for $0.5m_b \le \mu \le 1.5m_b$.

(4) For the case of $l^- = (e^-, \mu^-)$, the PQCD and PQCD + Lattice predictions for the values of P_L are very similar and close to -1 in value. For the τ^- lepton, however, the PQCD and PQCD + Lattice predictions for P_L show a moderate difference: -0.35 against -0.24.

C. Observables for $B_s \to K^* \ell^+ \ell^-$

Analogous to the cases of $B_s \to K \ell^+ \ell^-$ decays, we follow the same procedure to calculate the physical observables of $B_s \to K^* \ell^+ \ell^-$ by using the PQCD and PQCD + Lattice approaches, respectively. For $B_s \to K^* \ell^+ \ell^-$ decays, however, many more physical observables are defined and studied.

In Table XI we listed the PQCD and PQCD + Lattice predictions for the branching ratios $\mathcal{B}(\bar{B}_s \to K^* \ell^+ \ell^-)$ and $\mathcal{B}(B_s \to \bar{K}^* \ell^+ \ell^-)$ with $l = (e, \mu, \tau)$, the lepton forward-backward asymmetries $\mathcal{A}_{FB}$, the longitudinal polarization asymmetries $F_L^{K^*}$ of the leptons, the direct CP asymmetries $\mathcal{A}_{CP}$, and the ratios of the branching ratios $R_{K^*}^{e\mu}$ and $R_{K^*}^{\mu\tau}$ with the choice of the scale $\mu = m_b$. In numerical calculations, here we use the mean value of decay rate $\Gamma_{B_s^0} = 1.509 \times 10^{12}\ \text{s}^{-1}$ [30]. For the branching ratios, the extra error from the S-wave pollution up to 10% should also be added [32]. In Table XII we listed the PQCD and PQCD + Lattice predictions for the values of those angular observables P_i $(i = 1, 2, 3)$ and P_j' $(j = 4, 5, 6, 8)$ in $l = (e, \mu, \tau)$ mode. The total errors of all theoretical predictions in Tables XI and XII are estimated in the same way as that for the case of $\bar{B}_s \to K l^+ l^-$ decays.

From Table XI, it is easy to find the CP-averaged branching ratio $\mathcal{B}(\bar{B}_s \to K^* l^+ l^-)$ for $l = (e, \mu, \tau)$:

TABLE XI. The PQCD and PQCD + Lattice predictions for the branching ratios (in unit of 10^{-8}) of the semileptonic decays $B_s \to K^* \ell^+ \ell^-$, the lepton forward-backward asymmetry $\mathcal{A}_{FB}$, the K^* polarization fraction $F_L^{K^*}$, the direct CP asymmetry $\mathcal{A}_{CP}$ (in unit of 10^{-2}), and the ratios $R_{K^*}^{e\mu}$ and $R_{K^*}^{\mu\tau}$. The theoretical errors from the input parameters are combined in quadrature.

		PQCD		PQCD + Lattice	
Mode	Observables	$\bar{B}_s \to K^* \ell^+ \ell^-$	$B_s \to \bar{K}^* \ell^+ \ell^-$	$\bar{B}_s \to K^* \ell^+ \ell^-$	$B_s \to \bar{K}^* \ell^+ \ell^-$
$\ell = e$	$\mathcal{B}$	$3.74^{+1.38}_{-1.16}$	$3.68^{+1.33}_{-1.14}$	$3.00^{+0.91}_{-0.76}$	$2.99^{+0.94}_{-0.78}$
	$\mathcal{A}_{FB}$	$-0.244(9)$	$-0.235(17)$	$-0.183(10)$	$-0.176(10)$
	$F_L^{K^*}$	0.373(2)	0.393(5)	0.408(7)	0.432(9)
	$\mathcal{A}_{CP}$	0.8 ± 0.3		0.2 ± 0.4	
$\ell = \mu$	$\mathcal{B}$	$3.20^{+1.26}_{-1.00}$	$3.14^{+1.19}_{-0.98}$	$2.48^{+0.67}_{-0.59}$	$2.47^{+0.70}_{-0.61}$
	$\mathcal{A}_{FB}$	$-0.285(17)$	$-0.275(14)$	$-0.222(6)$	$-0.214(6)$
	$F_L^{K^*}$	0.434(12)	0.457(16)	0.494(16)	0.522(18)
	$\mathcal{A}_{CP}$	1.0 ± 0.5		0.2 ± 0.5	
$\ell = \tau$	$\mathcal{B}$	$0.71^{+0.35}_{-0.21}$	$0.72^{+0.36}_{-0.21}$	0.49 ± 0.09	0.50 ± 0.09
	$\mathcal{A}_{FB}$	$-0.235(33)$	$-0.232(33)$	$-0.196(5)$	$-0.194(5)$
	$F_L^{K^*}$	0.420(13)	0.418(13)	0.480(5)	0.478(5)
	$\mathcal{A}_{CP}$	-0.7 ± 0.3		-1.0 ± 0.2	
	$R_{K^*}^{e\mu}$	0.993(2)	0.993(2)	0.992(2)	0.992(2)
	$R_{K^*}^{\mu\tau}$	0.227(30)	0.238(35)	0.205(20)	0.211(22)

TABLE XII. The PQCD and PQCD + Lattice predictions for the angular observables P_i ($i = 1, 2, 3$) and P'_j ($j = 4, 5, 6, 8$) of the decays $\bar{B}_s \to K^*\ell^+\ell^-$ (the first row) and $B_s \to \bar{K}^*\ell^+\ell^-$ (the second row). The total uncertainties of the input parameters are combined in quadrature.

	e Mode		μ Mode		τ Mode	
Obs.	PQCD	PQCD + Lattice	PQCD	PQCD + Lattice	PQCD	PQCD + Lattice
$-P_1$	0.34 ± 0.12	0.37 ± 0.05	0.44 ± 0.12	0.52 ± 0.04	0.62 ± 0.12	0.68 ± 0.02
	0.33 ± 0.11	0.36 ± 0.05	0.44 ± 0.12	0.52 ± 0.04	0.62 ± 0.12	0.68 ± 0.02
$-P_2$	0.27 ± 0.01	0.21 ± 0.01	0.34 ± 0.03	0.30 ± 0.01	0.36 ± 0.05	0.35 ± 0.01
	0.26 ± 0.01	0.21 ± 0.01	0.35 ± 0.03	0.31 ± 0.01	0.36 ± 0.05	0.35 ± 0.01
$-P_3 \times 10^3$	0.17 ± 1.17	0.34 ± 0.21	0.19 ± 1.43	0.45 ± 0.29	0.35 ± 0.99	0.91 ± 0.13
	1.27 ± 0.99	2.84 ± 0.51	1.68 ± 1.15	4.11 ± 0.52	0.38 ± 1.08	0.98 ± 0.14
P'_4	1.06 ± 0.07	1.06 ± 0.04	1.10 ± 0.07	1.11 ± 0.03	1.27 ± 0.05	1.29 ± 0.01
	1.00 ± 0.01	0.99 ± 0.04	1.07 ± 0.07	1.07 ± 0.03	1.27 ± 0.05	1.29 ± 0.01
$-P'_5$	0.57 ± 0.06	0.48 ± 0.02	0.61 ± 0.07	0.52 ± 0.02	0.58 ± 0.10	0.54 ± 0.01
	0.57 ± 0.05	0.48 ± 0.02	0.61 ± 0.06	0.53 ± 0.02	0.57 ± 0.10	0.54 ± 0.01
$-P'_6 \times 10^3$	0.76 ± 0.15	0.96 ± 0.09	0.68 ± 0.13	0.87 ± 0.08	0.11 ± 0.03	0.12 ± 0.01
	0.77 ± 0.14	0.96 ± 0.08	0.70 ± 0.13	0.87 ± 0.07	0.11 ± 0.02	0.12 ± 0.01
$-P'_8 \times 10^2$	0.61 ± 0.06	0.67 ± 0.07	-0.36 ± 0.27	-0.57 ± 0.26	0.27 ± 0.07	0.37 ± 0.03
	1.33 ± 0.09	1.70 ± 0.06	2.20 ± 0.27	2.83 ± 0.26	0.30 ± 0.07	0.39 ± 0.03

$$\mathcal{B}(\bar{B}_s \to K^* e^+ e^-)|_{\text{CP-av.}} = \begin{cases} (3.71^{+0.98}_{-0.82} \pm 0.37) \times 10^{-8}, & \text{PQCD}, \\ (3.00^{+0.66}_{-0.55} \pm 0.30) \times 10^{-8}, & \text{PQCD + Lattice}, \end{cases} \tag{104}$$

$$\mathcal{B}(\bar{B}_s \to K^* \mu^+ \mu^-)|_{\text{CP-av.}} = \begin{cases} (3.17^{+0.89}_{-0.71} \pm 0.32) \times 10^{-8}, & \text{PQCD}, \\ (2.48^{+0.50}_{-0.43} \pm 0.25) \times 10^{-8}, & \text{PQCD + Lattice}, \end{cases} \tag{105}$$

$$\mathcal{B}(\bar{B}_s \to K^* \tau^+ \tau^-)|_{\text{CP-av.}} = \begin{cases} (0.72^{+0.25}_{-0.17} \pm 0.07) \times 10^{-8}, & \text{PQCD}, \\ (0.50 \pm 0.06 \pm 0.05) \times 10^{-8}, & \text{PQCD + Lattice}. \end{cases} \tag{106}$$

where the second errors come from the 10% S-wave pollution as estimated in Ref. [32].

In Fig. 6, we show the PQCD and the PQCD + Lattice predictions of q^2 dependence of the differential decay rate $d\mathcal{B}/dq^2$, the forward-backward asymmetry $\mathcal{A}_{FB}(q^2)$, the longitudinal polarization $F_L^{K^*}(q^2)$ for $B_s \to K^*\ell^+\ell^-$ decays with $\ell = (\mu, \tau)$, $q^2_{\text{max}} = 20.02\ \text{GeV}^2$, and the renormalization scale $\mu = m_b$. The red (blue) lines (dashed lines) correspond to the predictions obtained using the PQCD (PQCD + Lattice) approach, while the shaded narrow bands (red and blue) indicate the uncertainty of our predictions due to the variations of the input parameters. For the cases of the decays $B_s \to K^*\mu^+\mu^-$, the two vertical grey blocks show the experimental veto regions [1] in order to remove the contributions from the resonance $J/\psi(1S)$ (left-hand band) and $\psi'(2S)$ (right-hand band) to the form factor dependent observables. For the case of the decay $B_s \to K^*\tau^+\tau^-$, on the other hand, there is one vertical grey block which shows the experimental veto region [1] for the resonance $\psi'(2S)$ only.

In Figs. 7 and 8, we show the q^2 dependence of the angular observables P_i ($i = 1, 2, 3$) and P'_j ($j = 4, 5, 6, 8$) for the considered semileptonic decays $B_s \to K^* l^+ l^-$ with $\ell = (\mu, \tau)$, respectively. Since the relevant figures for the electron mode are very similar with those for the muon mode, we do not draw them in Figs. 6–8. The symbols in these two figures have the same meaning as those in Fig. 5.

From the numerical predictions as given in Tables XI and XII and in Figs. 6–8, we find the following points about the physical observables of the $\bar{B}_s \to K^* l^+ l^-$ ($\ell = e, \mu, \tau$) decays:

(1) For the considered decay modes, the PQCD and PQCD + Lattice predictions for $\mathcal{B}(\bar{B}_s \to K^* l^+ l^-)$ with $\ell = (e, \mu, \tau)$ do agree well with each other within the errors. The PQCD + Lattice predictions of $\mathcal{B}(\bar{B}_s \to K^* l^+ l^-)$ have smaller errors than those of the PQCD predictions. Both PQCD and PQCD + Lattice predictions of $\mathcal{B}(\bar{B}_s \to K^* \mu^+ \mu^-)$ do agree well with the LCSR prediction $(2.85 \pm 0.72) \times 10^{-8}$ [29] and with the currently available LHCb measured value $(2.9 \pm 1.1) \times 10^{-8}$ [20]. For the electron and muon modes, on the other hand, we have to wait for the future experimental measurements.

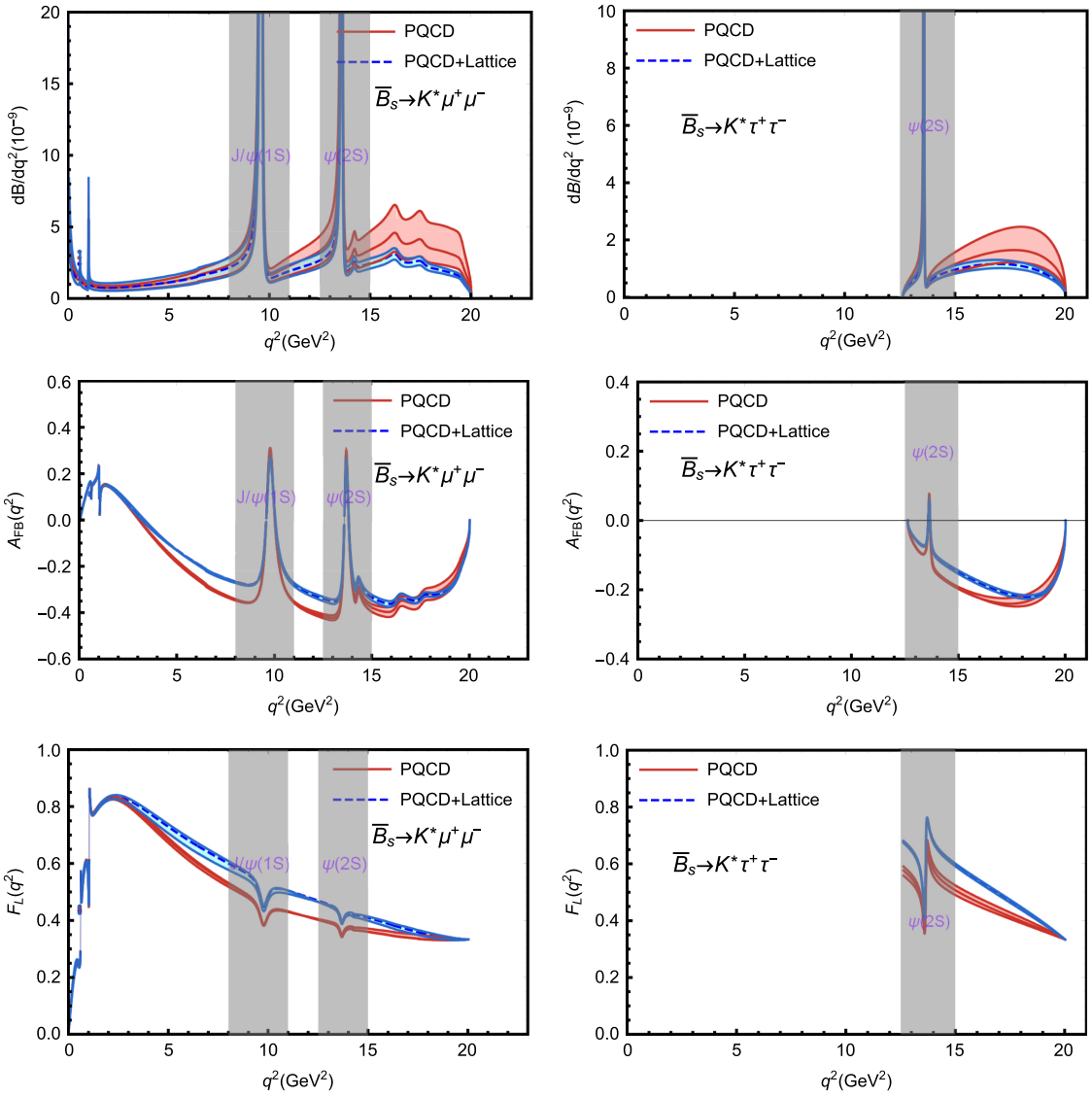

FIG. 6. The theoretical predictions for the q^2 dependence of $d\mathcal{B}/dq^2$, $\mathcal{A}_{FB}(q^2)$, and $F_L^{K^*}(q^2)$ for the decays $\bar{B}_s \to K^* \ell^+ \ell^-$ with $\ell = (\mu, \tau)$ in the PQCD and PQCD + Lattice approaches. For more details see the text.

(2) For the ratio $R_{K^*}^{e\mu}$, the theoretical predictions from both PQCD and PQCD + Lattice approaches are almost the same one, with a tiny ∼1% error because of the great cancellation of the errors in the ratio of the branching ratios. For the ratio $R_{K^*}^{\mu\tau}$, however, the remaining error of the theoretical predictions from both PQCD and PQCD + Lattice approaches are still around 10%. These two ratios should be measured in the future experiments.

(3) For the direct CP asymmetries $\mathcal{A}_{CP}$ of the considered decays, they are always very small as expected: less than 2% in magnitude. For physical observables $\mathcal{A}_{FB}$ and $F_L^{K^*}$, the differences between the central values of the PQCD and PQCD + Lattice are about 20% in magnitude, while the errors of the theoretical predictions are less than 10%.

(4) For the angular observables P_i and P_j', the PQCD and PQCD + Lattice predictions for each mode are consistent within errors. The values of P_3 and $P_{6,8}'$ are close to zero: $\sim 10^{-2}$ for P_8' and $\sim 10^{-3}$ for P_3 and P_6'. For the remaining $P_{1,2}$ and $P_{4,5}'$, their magnitudes are small: $-1 < (P_{1,2}, P_5') < -0.2$ while $P_4' \sim 1$.

(5) One can see from the curves in Figs. 7 and 8 that most angular observables P_i and P_j' have weak q^2 dependence in the major region of q^2 due to the large cancellation of q^2 dependence in the ratios.

For the semileptonic decays $\bar{B}_s \to K^* \ell^+ \ell^-$ ($\ell = e, \mu$), some regions of q^2 do correspond to some resonance states, such as the charmonium $J/\Psi, \psi(2S)$, etc., and should be removed for the sake of data analysis. Following Ref. [29],

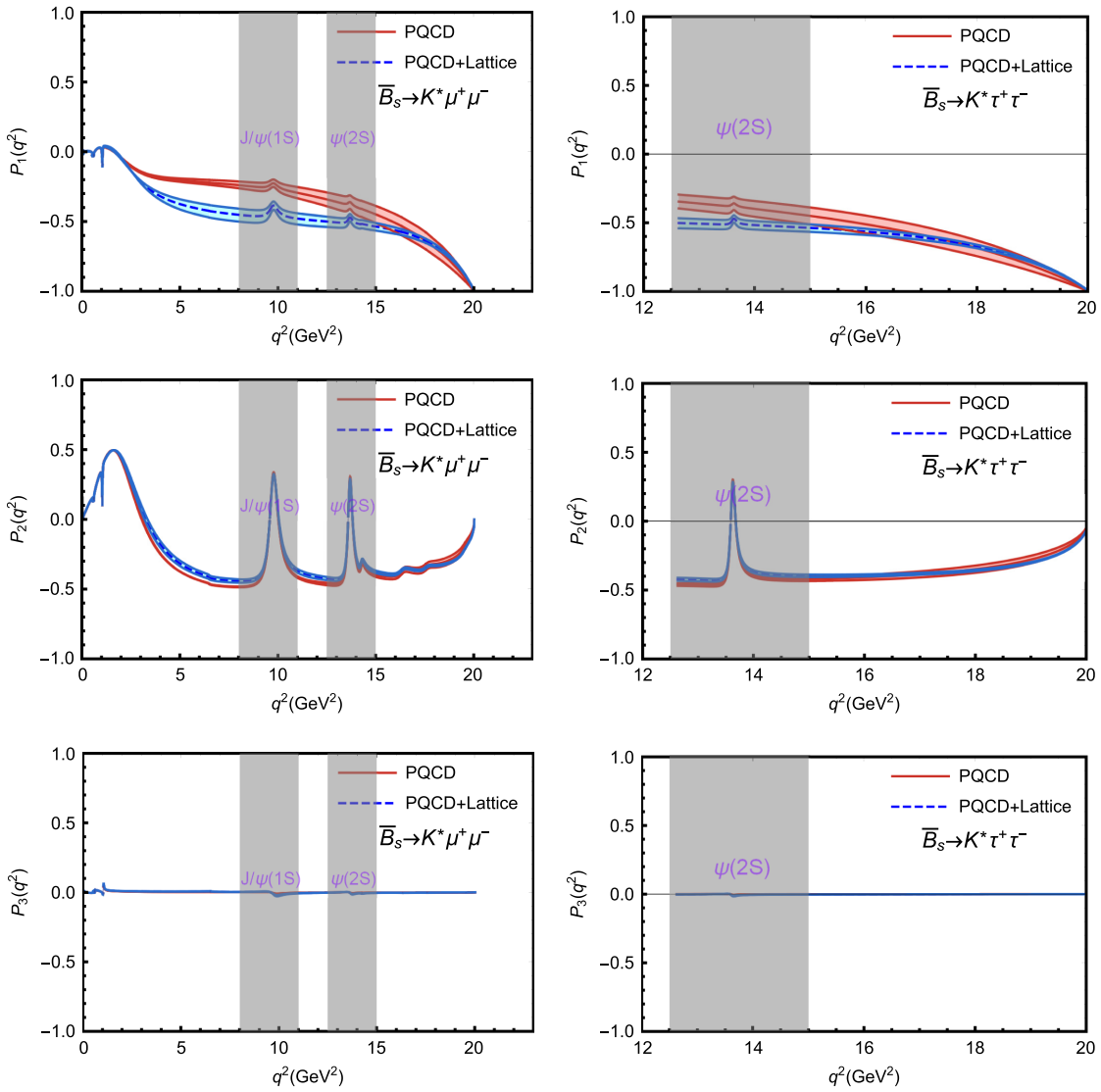

FIG. 7. The theoretical predictions for the q^2 dependence of the angular observables P_i ($i = 1, 2, 3$) for the decays $\bar{B}_s \to K^* l^+ l^-$ ($\ell = \mu, \tau$) in the PQCD and PQCD + Lattice approaches. For details see the text.

we here also present the binned value of the observables as a function of lepton-pair momentum q^2 covering two q^2 regions: [0.1–0.98] GeV^2 and [1.1–6] GeV^2 and consider the mass effect in the final state. We employ the PQCD and PQCD + Lattice approach to evaluate the form factors and compare the resultant results. Analogous to Ref. [29], we also define the q^2-binned observables in the following form:

$$\langle P_1\rangle_{bin} = \frac{\int_{bin} dq^2(I_3)}{2\int_{bin} dq^2(I_2^s)}, \qquad \langle P_2\rangle_{bin} = \frac{\int_{bin} dq^2(\beta_\ell I_6^s)}{8\int_{bin} dq^2(I_2^s)}, \qquad \langle P_3\rangle_{bin} = -\frac{\int_{bin} dq^2(I_9)}{4\int_{bin} dq^2(I_2^s)}, \tag{107}$$

$$\langle P_4'\rangle_{bin} = \frac{\int_{bin} dq^2(I_4)}{\sqrt{-\int_{bin} dq^2(I_2^c I_2^s)}}, \qquad \langle P_5'\rangle_{bin} = \frac{\int_{bin} dq^2(\beta_\ell I_5)}{2\sqrt{-(\int_{bin} dq^2(I_2^c I_2^s))}}, \tag{108}$$

$$\langle P_6'\rangle_{bin} = -\frac{\int_{bin} dq^2(\beta_\ell I_7)}{2\sqrt{-(\int_{bin} dq^2(I_2^c I_2^s))}}, \qquad \langle P_8'\rangle_{bin} = -\frac{\int_{bin} dq^2(I_8)}{\sqrt{-(\int_{bin} dq^2(I_2^c I_2^s))}}, \tag{109}$$

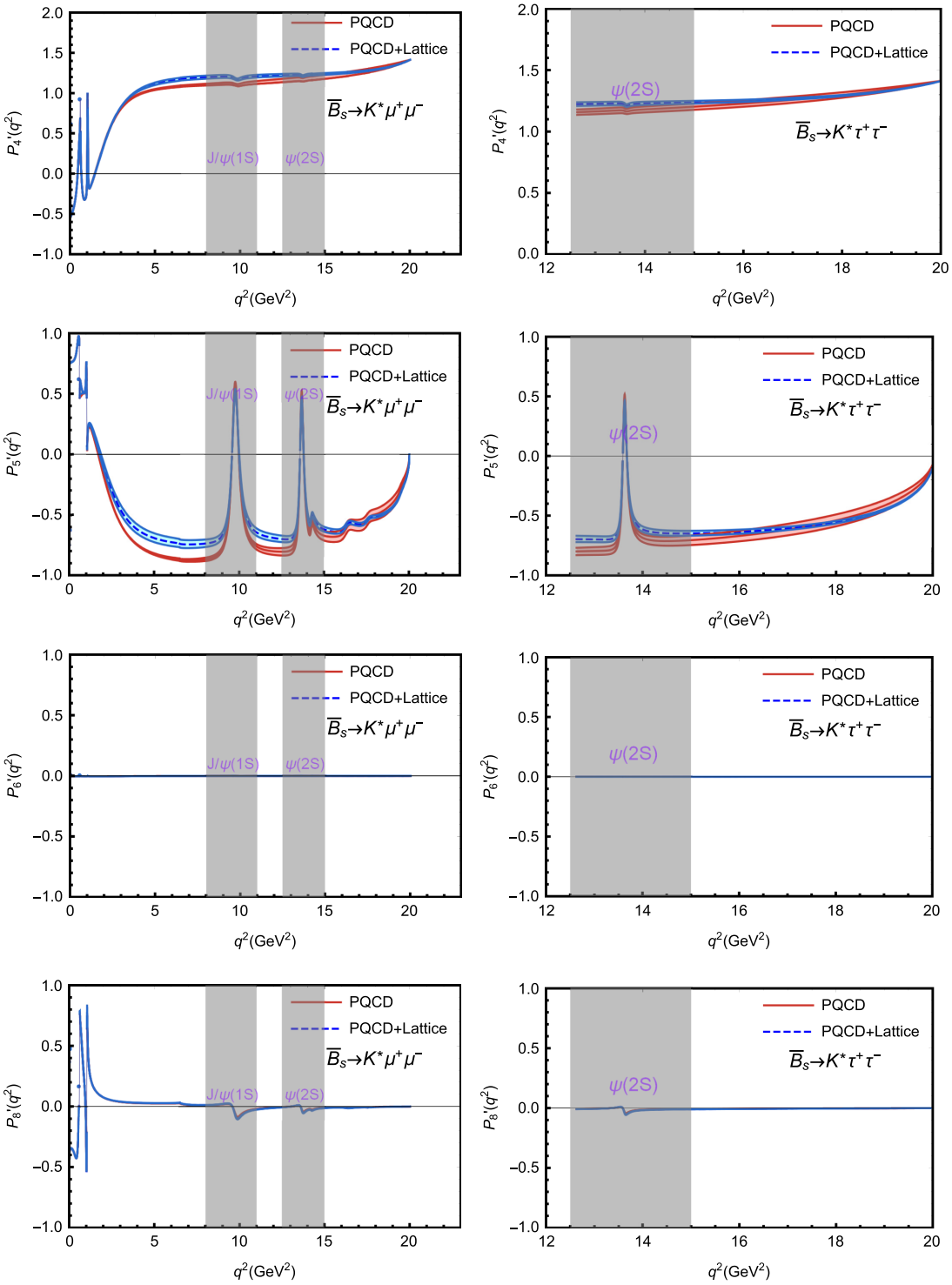

FIG. 8. The theoretical predictions for the q^2 dependence of the angular observables P_j' ($j = 4, 5, 6, 8$) for the decays $\bar{B}_s \to K^* l^+ l^-$ ($\ell = \mu, \tau$) in the PQCD and PQCD + Lattice approaches. For details see the text.

$$\langle \mathcal{B} \rangle_{bin} = \int_{bin} dq^2 \frac{d\mathcal{B}(B_s \to K^* \ell^+ \ell^-)}{dq^2}, \quad (110)$$

$$\langle R_{K^*} \rangle_{bin} = \frac{\langle BR \rangle_{bin}(\ell = \mu)}{\langle BR \rangle_{bin}(\ell = e)}, \quad (111)$$

$$\langle \mathcal{A}_{\mathrm{FB}}(\ell) \rangle_{bin} = \frac{\int_{bin} dq^2 b_{\theta_\ell}(q^2)}{\int_{bin} dq^2 d\Gamma/dq^2} = \frac{3 \int_{bin} dq^2 I_6^s}{4\Gamma_{bin}}, \quad (112)$$

$$\langle F_L^{K^*} \rangle_{bin} = \frac{3 \int_{bin} dq^2 (I_1^c - I_2^c)}{\int_{bin} dq^2 [3(I_1^c + 2I_1^s) - (I_2^c + 2I_2^s)]}. \quad (113)$$

TABLE XIII. The binned values of observables for the process $\bar{B}_s \to K^*\mu^+\mu^-$ and $B_s \to \bar{K}^*\mu^+\mu^-$ at $\mu = m_b$ scale using the PQCD and PQCD + Lattice factorization approaches. The uncertainties shown are due to errors in determination of form factors and CKM parameters. The LCSR predictions for $B_s \to K^*\mu^+\mu^-$ decay as given in Ref. [29] were added as a comparison. For details see the text.

		$\bar{B}_s \to K^*\mu^+\mu^-$		$B_s \to \bar{K}^*\mu^+\mu^-$	
Decay Mode	Observables/Bin	[0.1–0.98] GeV^2	[1.1–6] GeV^2	[0.1–0.98] GeV^2	[1.1–6] GeV^2
$\langle P_1 \rangle$	PQCD	0.004(2)	−0.157(16)	0.023(2)	−0.163(16)
	PQCD + Lattice	0.003(2)	−0.279(25)	0.021(3)	−0.292(28)
	LCSR [29]	0.012(129)	−0.081(111)	0.011(135)	−0.075(108)
$\langle P_2 \rangle$	PQCD	0.127(2)	−0.127(6)	0.139(2)	−0.223(5)
	PQCD + Lattice	0.128(2)	−0.101(18)	0.141(2)	−0.155(16)
	LCSR [29]	0.118(13)	0.112(80)	0.112(13)	0.142(79)
$\langle P_3 \rangle \times 10^2$	PQCD	0.1 ± 0.1	0.4 ± 0.2	0.2 ± 0.2	0.5 ± 0.2
	PQCD + Lattice	0.1 ± 0.1	0.8 ± 0.2	0.2 ± 0.2	0.9 ± 0.2
	LCSR [29]	0.1 ± 0.2	0.4 ± 1.0	0.1 ± 0.7	0.3 ± 1.0
$\langle P_4' \rangle$	PQCD	−0.131(2)	0.817(14)	−0.603(2)	0.849(13)
	PQCD + Lattice	−0.131(3)	0.854(7)	−0.604(3)	0.890(9)
	LCSR [29]	−0.593(58)	0.464(165)	−0.650(60)	0.379(172)
$\langle P_5' \rangle$	PQCD	0.711(3)	−0.608(3)	0.394(2)	−0.650(4)
	PQCD + Lattice	0.715(2)	−0.486(40)	0.392(2)	−0.524(39)
	LCSR [29]	0.547(53)	−0.286(133)	0.543(55)	−0.273(140)
$\langle P_6' \rangle \times 10^2$	PQCD	-0.4 ± 0.2	-0.2 ± 0.2	-0.3 ± 0.2	-0.2 ± 0.2
	PQCD + Lattice	-0.3 ± 0.5	-0.2 ± 0.2	-0.3 ± 0.2	-0.2 ± 0.2
	LCSR [29]	-10.4 ± 1.7	-9.5 ± 1.1	-6.9 ± 0.5	-7.8 ± 0.4
$\langle P_8' \rangle$	PQCD	0.042(2)	0.050(2)	0.044(2)	0.057(2)
	PQCD + Lattice	0.041(2)	0.053(2)	0.045(2)	0.062(2)
	LCSR [29]	0.015(16)	0.040(17)	0.044(16)	0.034(19)
$\langle \mathcal{B} \rangle \times 10^9$	PQCD	1.44 ± 0.47	$4.65^{+1.52}_{-1.39}$	$1.72^{+0.69}_{-0.49}$	$4.99^{+2.09}_{-1.65}$
	PQCD + Lattice	$1.43^{+0.48}_{-0.42}$	$4.64^{+1.54}_{-1.41}$	$1.71^{+0.66}_{-0.48}$	$4.98^{+2.13}_{-1.71}$
	LCSR [29]	3.81 ± 0.46	7.80 ± 1.79	4.41 ± 0.57	8.39 ± 1.89
$\langle R_{K^*} \rangle$	PQCD	0.983(1)	0.995(1)	0.984(1)	0.996(1)
	PQCD + Lattice	0.982(1)	0.996(1)	0.984(1)	0.997(1)
	LCSR [29]	0.940(9)	0.998(4)	0.942(8)	0.998(4)
$\langle A_{FB}(\ell) \rangle$	PQCD	0.110(2)	−0.067(5)	0.076(2)	−0.087(5)
	PQCD + Lattice	0.110(2)	−0.034(4)	0.077(2)	−0.053(3)
	LCSR [29]	−0.060(8)	−0.029(22)	−0.056(8)	−0.036(22)
$\langle F_L^{K^*} \rangle$	PQCD	0.297(5)	0.741(11)	0.543(8)	0.738(10)
	PQCD + Lattice	0.297(10)	0.769(16)	0.543(13)	0.769(16)
	LCSR [29]	0.453(68)	0.853(39)	0.464(65)	0.851(39)

In Table XIII, we listed the PQCD and PQCD + Lattice predictions for the binned values of all eleven physical observables considered in this paper for the $\bar{B}_s \to K^*\mu^+\mu^-$ and the $B_s \to \bar{K}^*\mu^+\mu^-$ decays. The theoretical errors from the input parameters are combined in quadrature in the tabulated error estimates. As a comparison, we also insert an extra row of the results from the LCSR approach [29] into the table, for each physical observable. It is necessary to note that there exist three differences between our predictions and the LCSR results as given in Ref. [29]:

(1) The sign definition of the forward-backward asymmetry A_{FB} in Ref. [29] is opposite to ours as given in Eq. (76).
(2) Our choices of the q^2 bin are [0.1–0.98] GeV^2 and [1.1–6] GeV^2, instead of the [0.1–1] GeV^2 and [1–6] GeV^2 in Ref. [29], because we try to remove the possible contribution from the light resonance $\phi(1020)$.
(3) The authors in Ref. [29] considered the nonfactorizable corrections like weak annihilation and spectator scattering in the bin [1–6] GeV^2 while these

effects in our analysis are very small and have been neglected.

On the theoretical side, from the numerical results as listed in Table XIII, one can find the following points:

(1) For binned values of observables $\langle P_{1,2}\rangle$ and $\langle A_{FB}(\ell)\rangle$, the differences between the PQCD and PQCD + Lattice predictions are around (20–40)% of the central values. For other eight physical observables, however, the PQCD and PQCD + Lattice predictions agree very well within errors. The source of the difference comes from a little different q^2 dependence of the form factors of these two factorization approaches.

(2) The differences between our results and LCSR predictions [29] are generally not large in magnitude and could be understood if one takes the three differences between our approaches and the LCSR as specified in the previous paragraph. Current differences will be tested in the future when the experimental measurements become available.

(3) For observables $\langle P_3\rangle$ and $\langle P'_{6,8}\rangle$, their SM values are tiny, about 10^{-3} to 10^{-2} in magnitude, because they are basically driven by the NLO contributions. It is noted that the observable P'_6 stems from the absorptive part of $b \to d\gamma$, a small imaginary number. Since these observables are not protected from hadronic uncertainties in general, their values are more sensitive to the choice of the method of calculating the form factors or to the variations of the input parameters being used in calculations.

(4) In this paper, the possible long-distance charm-loop effects have been taken into account. The modification induced to C_9 is encoded in a shift where the factorizable charm loop and nonfactorizable soft gluon are taken into account. We also use a phenomenological model to account for light resonances like $\rho(770)$ and $\omega(782)$ in the low-q^2 region. It is interesting to note that such a particular effect is difficult to estimate and can be large in size, casting some doubts on the possibility to exploit the bins between J/ψ and $\psi(2S)$ for comparison with experiments.

VI. SUMMARY AND CONCLUSIONS

In the framework of the SM, here we studied the rare semileptonic decays $\bar{B}_s \to K^{(*)}\ell^+\ell^-$ with $l^- = (e^-, \mu^-, \tau^-)$ by using the PQCD and PQCD + Lattice factorization approaches and provided the theoretical predictions for the thirteen kinds of physical observables: the branching ratios $\mathcal{B}(\bar{B}_s \to K^{(*)}\ell^+\ell^-)$, $\mathcal{B}(B_s \to \bar{K}^{(*)}\ell^+\ell^-)$ and their CP averages, the ratios of the branching ratios $R^{e\mu}_{K,K^*}$ and $R^{\mu\tau}_{K,K^*}$, the lepton FB asymmetry $\mathcal{A}_{FB}(l)$, the longitudinal polarization asymmetry of the leptons P_L and the quantity $F_L^{K^*}$, the angular observables P_i with $(i=1,2,3)$, and P'_j with $(j = 4, 5, 6, 8)$. In the PQCD factorization approach, specifically, we first evaluated the relevant form factors $F_{0,+,T}(q^2)$, $V(q^2)$, $A_{0,1,2}(q^2)$ and $T_{1,2,3}(q^2)$ in the low-q^2 region and then extrapolate them to the whole q^2 region using the BCL parametrization method. In the PQCD + Lattice approach, we also take those currently available lattice QCD results for the relevant form factors at the end point $q^2_{\rm max}$ as additional input to improve the extrapolation of the form factors from the low-q^2 region to the whole range of q^2.

Based on our numerical calculations and the phenomenological analysis, we find the following main points:

(1) For all physical observables considered in this paper, the PQCD and PQCD + Lattice predictions do agree well within 1 standard deviation. The theoretical errors of the PQCD + Lattice predictions for the branching ratios become much smaller than those of the PQCD predictions.

(2) For $\bar{B}_s \to (K, K^*)\mu^+\mu^-$ decays, for example, the PQCD and PQCD + Lattice predictions for the CP-averaged branching ratios are the following:

$$\mathcal{B}(\bar{B}_s \to K\mu^+\mu^-)|_{\text{CP-av.}} = \begin{cases} (1.28^{+0.52}_{-0.48}) \times 10^{-8}, & \text{PQCD}, \\ (1.06^{+0.22}_{-0.29}) \times 10^{-8}, & \text{PQCD + Lattice}, \end{cases} \tag{114}$$

$$\mathcal{B}(\bar{B}_s \to K^*\mu^+\mu^-)|_{\text{CP-av.}} = \begin{cases} (3.17^{+0.95}_{-0.78}) \times 10^{-8}, & \text{PQCD}, \\ (2.48^{+0.56}_{-0.50}) \times 10^{-8}, & \text{PQCD + Lattice}. \end{cases} \tag{115}$$

Our theoretical predictions for the $\mathcal{B}(\bar{B}_s \to K^*\mu^+\mu^-)$ do agree well with the measured one $(2.9 \pm 1.1) \times 10^{-8}$ as reported by the LHCb Collaboration [20].

(3) For the ratios $R^{e\mu}_{K^*}$ and $R^{\mu\tau}_{K^*}$, the PQCD and PQCD + Lattice predictions agree very well and have a small error less than 10% due to the cancellation of the theoretical uncertainties in the ratios of the branching ratios. For the direct CP asymmetries $\mathcal{A}_{CP}$, they are always very small: less than 5% in magnitude. For physical observables $\mathcal{A}_{FB}$ and $F_L^{K^*}$, the differences between the central values of the PQCD and PQCD + Lattice are about $(10 \sim 30)$% in magnitude, while the errors of the theoretical predictions are less than 10%.

(4) For the angular observables $P_{1,2,3}$ and $P'_{4,5,6,8}$, the PQCD and PQCD + Lattice predictions for each lepton l^- are consistent within errors. The theoretical predictions of P_3 and $P'_{6,8}$ are tiny, say less than 10^{-2} in absolute value, and thus hardly to be measured. For the remaining $P_{1,2}$ and $P'_{4,5}$, on the other hand,

their magnitudes are larger than 0.2 and therefore could be measured by future LHCb and Belle-II experiments.

(5) For the sake of data analysis, we also defined eleven q^2-binned observables and presented our theoretical predictions of the binned values of all considered observables with the choice of two q^2 bins $[0.1\text{–}0.98]\ \mathrm{GeV}^2$ and $[1.1\text{–}6]\ \mathrm{GeV}^2$. The PQCD and PQCD + Lattice predictions generally agree with each other and are also consistent with most LCSR results within errors.

In general, we believe that most physical observables considered in this paper could be measured in the future LHCb or Belle-II experiments. Any clear deviations from above SM predictions might be a signal of new physics beyond the SM.

ACKNOWLEDGMENTS

This work was supported by the National Natural Science Foundation of China under Grants No. 11775117 and No. 11235005.

APPENDIX: RELEVANT FUNCTIONS

The threshold resummation factor $S_t(x)$ is adopted from [76]:

$$S_t = \frac{2^{1+2c}\Gamma(3/2+c)}{\sqrt{\pi}\Gamma(1+c)}[x(1-x)]^c, \tag{A1}$$

and here we set the parameter $c = 0.3$. The hard functions h_1 and h_2 come form the Fourier transform and can be written as

$$h_1(x_1,x_2,b_1,b_2) = K_0(\beta_1 b_1)[\theta(b_1-b_2)I_0(\alpha_1 b_2)K_0(\alpha_1 b_1) + \theta(b_2-b_1)I_0(\alpha_1 b_1)K_0(\alpha_1 b_2)]S_t(x_2), \tag{A2}$$

$$h_2(x_1,x_2,b_1,b_2) = K_0(\beta_2 b_1)[\theta(b_1-b_2)I_0(\alpha_2 b_2)K_0(\alpha_2 b_1) + \theta(b_2-b_1)I_0(\alpha_2 b_1)K_0(\alpha_2 b_2)]S_t(x_2), \tag{A3}$$

where K_0 and I_0 are modified Bessel functions, and

$$\alpha_1 = m_{B_s}\sqrt{x_2 r\eta^+}, \qquad \alpha_2 = m_{B_s}\sqrt{x_1 r\eta^+ - r^2 + r_d^2},$$
$$\beta_1 = \beta_2 = m_{B_s}\sqrt{x_1 x_2 r\eta^+}, \tag{A4}$$

where $r = m_{K^{(*)}}/m_{B_s}$, $r_d = m_d/m_{B_s}$.

The factor $\exp[-S_{ab}(t)]$ contains the Sudakov logarithmic corrections and the renormalization group evolution effects of both the wave functions and the hard scattering amplitude with $S_{ab}(t) = S_B(t) + S_M(t)$ [76],

$$S_B(t) = s\left(x_1\frac{m_{B_s}}{\sqrt{2}}, b_1\right) + \frac{5}{3}\int_{1/b_1}^{t}\frac{d\bar{\mu}}{\bar{\mu}}\gamma_q(\alpha_s(\bar{\mu})), \tag{A5}$$

$$S_M(t) = s\left(x_2\frac{m_{B_s}}{\sqrt{2}}r\eta^+, b_2\right) + s\left((1-x_2)\frac{m_{B_s}}{\sqrt{2}}r\eta^+, b_2\right) + 2\int_{1/b_2}^{t}\frac{d\bar{\mu}}{\bar{\mu}}\gamma_q(\alpha_s(\bar{\mu})), \tag{A6}$$

with the quark anomalous dimension $\gamma_q = -\alpha_s/\pi$. The explicit expressions of the functions $s(Q,b)$ can be found, for example, in Appendix A of Ref. [34]. The hard scales t_i in the above equation are chosen as the largest scale of the virtuality of the internal particles in the hard b-quark decay diagrams,

$$t_1 = \max\{\alpha_1, 1/b_1, 1/b_2\}, \qquad t_2 = \max\{\alpha_2, 1/b_1, 1/b_2\}. \tag{A7}$$

[1] J.-T. Wei *et al.* (Belle Collaboration), Measurement of the Differential Branching Fraction and Forward-Backword Asymmetry for $B \to K^{(*)}\ell^+\ell^-$, Phys. Rev. Lett. **103**, 171801 (2009).

[2] A. Ali, P. Ball, L. T. Handoko, and G. Hiller, A comparative study of the decays $B \to (K, K^*)\ell^+\ell^-$ in standard model and supersymmetric theories, Phys. Rev. D **61**, 074024 (2000).

[3] M. Beneke, T. Feldmann, and D. Seidel, Systematic approach to exclusive $B \to V\ell^+\ell^-$, $V\gamma$ decays, Nucl. Phys. **B612**, 25 (2001).

[4] C. H. Chen and C. Q. Geng, Exclusive decays of $B \to K^{(*)}\ell^+\ell^-$ in the PQCD, Phys. Rev. D **63**, 114025 (2001).

[5] A. Ali, G. Kramer, and G. h. Zhu, $B \to K^+\ell^+\ell^-$ decay in soft-collinear effective theory, Eur. Phys. J. C **47**, 625 (2006).

[6] U. Egede, T. Hurth, J. Matias, M. Ramon, and W. Reece, New observables in the decay mode $\bar{B}_d \to \bar{K}^{*0}\ell^+\ell^-$, J. High Energy Phys. 11 (2008) 032.

[7] C. Bobeth, G. Hiller, and G. Piranishvili, *CP* asymmetries in bar $B \to \bar{K}^*(\to \bar{K}\pi)\bar{\ell}\ell$ and untagged $\bar{B}_s$, $B_s \to \phi(\to K^+K^-)\bar{\ell}\ell$ decays at NLO, J. High Energy Phys. 07 (2008) 106.

[8] W. Altmannshofer, P. Ball, A. Bharucha, A. J. Buras, D. M. Straub, and M. Wick, Symmetries and asymmetries

of $B \to K^* \mu^+ \mu^-$ decays in the Standard Model and beyond, J. High Energy Phys. 01 (2009) 019.

[9] T. Aaltonen *et al.* (CDF Collaboration), Measurement of the Forward-Backward Asymmetry in the $B \to K^{(*)} \mu^+ \mu^-$ Decay and First Observation of the $B_s^0 \to \phi \mu^+ \mu^-$ Decay, Phys. Rev. Lett. **106**, 161801 (2011).

[10] J. P. Lees *et al.* (*BABAR* Collaboration), Measurement of branching fractions and rate asymmetries in the rare decays $B \to K^{(*)} l^+ l^-$, Phys. Rev. D **86**, 032012 (2012).

[11] R. Aaij *et al.* (LHCb Collaboration), Test of lepton universality using $B^+ \to K^+ \ell^+ \ell^-$ decays, Phys. Rev. Lett. **113**, 151601 (2014).

[12] V. Khachatryan *et al.* (CMS Collaboration), Angular analysis of the decay $B^0 \to K^{*0} \mu^+ \mu^-$ from pp collisions at $\sqrt{s} = 8$ TeV, Phys. Lett. B **753**, 424 (2016).

[13] R. Aaij *et al.* (LHCb Collaboration), Measurements of the S-wave fraction in $B^0 \to K^+ \pi^- \mu^+ \mu^-$ decays and the $B^0 \to K^*(892)^0 \mu^+ \mu^-$ differential branching fraction, J. High Energy Phys. 11 (2016) 047.

[14] R. Aaij *et al.* (LHCb Collaboration), Test of lepton universality with $B^0 \to K^{*0} \ell^+ \ell^-$ decays, J. High Energy Phys. 08 (2017) 055.

[15] R. Aaij *et al.* (LHCb Collaboration), Measurement of Form-Factor-Independent Observables in the Decay $B^0 \to K^{*0} \mu^+ \mu^-$, Phys. Rev. Lett. **111**, 191801 (2013).

[16] R. Aaij *et al.* (LHCb Collaboration), Angular analysis of the $B^0 \to K^{*0} \mu^+ \mu^-$ decay using 3 fb^{-1} of integrated luminosity, J. High Energy Phys. 02 (2016) 104.

[17] S. L. Glashow, J. Iliopoulos, and L. Maiani, Weak interactions with Lepton-Hadron symmetry, Phys. Rev. D **2**, 1285 (1970).

[18] M. Ciuchini, A. M. Coutinho, M. Fedele, E. Franco, A. Paul, L. Silvestrini, and M. Valli, On flavourful Easter eggs for new physics hunger and Lepton flavour universality violation, Eur. Phys. J. C **77**, 688 (2017).

[19] R. Aaij *et al.* (LHCb Collaboration), First measurement of the differential branching fraction and *CP* asymmetry of the $B^\pm \to \pi^\pm \mu^+ \mu^-$ decay, J. High Energy Phys. 10 (2015) 034.

[20] R. Aaij *et al.* (LHCb Collaboration), Evidence for the decay $B_s^0 \to \bar{K}^{*0} \mu^+ \mu^-$, J. High Energy Phys. 07 (2018) 020.

[21] J. J. Wang, R. M. Wang, Y. G. Xu, and Y. D. Yang, The rare decays $B_u^+ \to \pi^+ l^+ l^-, \rho^+ l^+ l^-$ and $B_d^0 \to l^+ l^-$ in the R-parity violating supersymmetry, Phys. Rev. D **77**, 014017 (2008).

[22] A. Ali, A. Ya. Parkhomenko, and A. V. Rusov, Precise calculation of the dilepton invariant-mass spectrum and the decay rate in $B^\pm \to \pi^\pm \mu^+ \mu^-$ in the SM, Phys. Rev. D **89**, 094021 (2014).

[23] W. S. Hou, M. Kohda, and F. Xu, Rates and asymmetries of $B \to \pi l^+ l^-$ decays, Phys. Rev. D **90**, 013002 (2014).

[24] C. Hambrock, A. Khodjamirian, and A. Rusov, Hadronic effects and observables in $B \to \pi l^+ l^-$ decay at large recoil, Phys. Rev. D **92**, 074020 (2015).

[25] J. A. Bailey *et al.* (Fermilab Lattice and MILC Collaborations), $B \to \pi l^+ l^-$ form Factors for New-Physics Searches from Lattice QCD, Phys. Rev. Lett. **115**, 152002 (2015).

[26] W. F. Wang and Z. J. Xiao, The semileptonic decays $B/B_s \to (\pi, K)(\ell^+ \ell^-, \ell \nu, \nu \bar{\nu})$ in the perturbative QCD approach beyond the leading-order, Phys. Rev. D **86**, 114025 (2012).

[27] W. F. Wang, Y. Y. Fan, M. Liu, and Z. J. Xiao, Semileptonic decays $B/B_s \to (\eta, \eta', G)(\ell^+ \ell^-, \ell \bar{\nu}, \nu \bar{\nu})$ in the perturbative QCD approach beyond the leading order, Phys. Rev. D **87**, 097501 (2013).

[28] A. Khodjamirian and A. V. Rusov, $B_s \to K \ell \nu_\ell$ and $B_{(s)} \to \pi(K) \ell^+ \ell^-$ decays at large recoil and CKM matrix elements, J. High Energy Phys. 08 (2017) 112.

[29] B. Kindra and N. Mahajan, Predictions of angular observables for $\bar{B}_s \to K^* \ell \ell$ and $\bar{B} \to \rho \ell \ell$ in the standard model, Phys. Rev. D **98**, 094012 (2018).

[30] M. Tanabashi *et al.* (Particle Data Group), Review of particle physics, Phys. Rev. D **98**, 030001 (2018).

[31] S. Aoki *et al.* (Flavour Lattice Averaging Group), FLAG Review 2019, Eur. Phys. J. C **80**, 113 (2020).

[32] M. Döring, U. G. Meißner, and W. Wang, Chiral dynamics and S-wave contributions in semileptonic B decays, J. High Energy Phys. 10 (2013) 011.

[33] Y. Y. Kim, H. N. Li, and A. I. Sanda, Penguin enhancement and $B \to K\pi$ decays in perturbative QCD, Phys. Rev. D **63**, 054008 (2001).

[34] C. D. Lu, K. Ukai, and M. Z. Yang, Branching ratio and *CP* violation of $B \to \pi\pi$ decays in the perturbative QCD approach, Phys. Rev. D **63**, 074009 (2001).

[35] H. N. Li, QCD Aspects of exclusive B meson decays, Prog. Part. Nucl. Phys. **51**, 85 (2003), and references therein.

[36] C. Bourrely, I. Caprini, and L. Lellouch, Model-independent description of $B \to \pi l \nu$ decays and a determination of $|V_{ub}|$, Phys. Rev. D **79**, 013008 (2009); Erratum, Phys. Rev. D **82**, 099902 (2010).

[37] D. Leljak, B. Melic, and M. Patra, On lepton flavour universality in semileptonic $B_c \to \eta_c, J/\Psi$ decays, J. High Energy Phys. 05 (2019) 094.

[38] Y. Y. Fan, W. F. Wang, S. Cheng, and Z. J. Xiao, Semileptonic decays $B \to D^{(*)} l \nu$ in the perturbative QCD factorization approach, Chin. Sci. Bull. **59**, 125 (2014).

[39] Z. J. Xiao, W. F. Wang, and Y. Y. Fan, Revisiting the pure annihilation decays $B_s \to \pi^+ \pi^-$ and $B^0 \to K^+ K^-$: The data and the pQCD predictions, Phys. Rev. D **85**, 094003 (2012).

[40] Y. Y. Fan, W. F. Wang, S. Cheng, and Z. J. Xiao, Anatomy of $B \to K \eta^{(\prime)}$ decays in different mixing schemes and effects of next-to-leading order contributions in the perturbative QCD approach, Phys. Rev. D **87**, 094003 (2013).

[41] D. C. Yan, P. Yang, X. Liu, and Z. J. Xiao, Anatomy of $B_s \to PV$ decays and effects of next-to-leading order contributions in the perturbative QCD factorization approach, Nucl. Phys. **B931**, 79 (2018).

[42] D. C. Yan, X. Liu, and Z. J. Xiao, Anatomy of $B_s \to VV$ decays and effects of next-to-leading order contributions in the perturbative QCD factorization approach, Nucl. Phys. **B935**, 17 (2018).

[43] P. Ball, V. M. Braun, and A. Lenz, Higher-twist distribution amplitudes of the K meson in QCD, J. High Energy Phys. 05 (2006) 004.

[44] A. Ali, G. Kramer, Y. Li, C. D. Lu, Y. L. Shen, W. Wang, and Y. M. Wang, Charmless non-leptonic B_s decays to PP, PV and VV final states in the pQCD approach, Phys. Rev. D **76**, 074018 (2007).

[45] R. H. Li, C. D. Lu, W. Wang, and X. X. Wang, $B \to S$ transition form factors in the PQCD approach, Phys. Rev. D **79**, 014013 (2009).

[46] S. R. Singh and B. Mawlong, 331-Z' mediated FCNC effects on $b \to d\mu^+\mu^-$ transitions, Int. J. Mod. Phys. A **33**, 1850225 (2018).

[47] P. Nayek, P. Maji, and S. Sahoo, Study of semileptonic decays $B \to \pi\ell^+\ell^-$ and $B \to \rho\ell^+\ell^-$ in nonuniversal Z model, Phys. Rev. D **99**, 013005 (2019).

[48] R. Khosravi, Form factors and branching ratios of the FCNC $B \to a_1\ell^+\ell^-$ decays, Eur. Phys. J. C **75**, 220 (2015).

[49] C. H. Chen and C. Q. Geng, Baryonic rare decays of $\Lambda(b) \to \Lambda\ell^+\ell^-$, Phys. Rev. D **64**, 074001 (2001).

[50] G. Buchalla, A. J. Buras, and M. E. Lautenbacher, Weak decays beyond leading logarithms, Rev. Mod. Phys. **68**, 1125 (1996).

[51] C. S. Lim, T. Morozumi, and A. I. Sanda, A prediction for $d\Gamma(b \to s\ell\bar{\ell})/dq^2$ including the long distance effects, Phys. Lett. B **218**, 343 (1989).

[52] N. G. Deshpande, J. Trampetic, and K. Panose, Resonance background to the decays $b \to s\ell^+\ell^-$, $B \to K^*\ell^+\ell^-$ and $B \to K\ell^+\ell^-$, Phys. Rev. D **39**, 1461 (1989).

[53] A. Ali, T. Mannel, and T. Morozumi, Forward backward asymmetry of dilepton angular distribution in the decay $b \to s\ell^+\ell^-$, Phys. Lett. B **273**, 505 (1991).

[54] P. J. O'Donnell and H. K. K. Tung, Resonance contributions to the decay $b \to s\ell^+\ell^-$, Phys. Rev. D **43**, R2067 (1991).

[55] M. Jezabek and J. H. Kuhn, Lepton spectra from heavy quark decay, Nucl. Phys. **B320**, 20 (1989).

[56] B. Grinstein, M. J. Savage, and M. B. Wise, $B \to X_s e^+e^-$ in the six quark model, Nucl. Phys. **B319**, 271 (1989).

[57] M. Misiak, The $b \to se^+e^-$ and $b \to s\gamma$ decays with next-to-leading logarithmic QCD corrections, Nucl. Phys. **B393**, 23 (1993); **B439**, 461(E) (1995).

[58] A. J. Buras and M. Munz, Effective Hamiltonian for $B \to X_s e^+e^-$ beyond leading logarithms in the NDR and HV schemes, Phys. Rev. D **52**, 186 (1995).

[59] A. Khodjamirian, T. Mannel, A. A. Pivovarov, and Y.-M. Wang, Charm-loop effect in $B \to K^{(*)}\ell^+\ell^-$ and $B \to K^*\gamma$, J. High Energy Phys. 09 (2010) 089.

[60] D. P. Du, A. X. El-Khadra, S. Gottlieb, A. S. Kronfeld, J. Laiho, E. Lunghi, R. S. Van de Water, and R. Zhou (Fermilab Lattice and MILC Collaborations), Phenomenology of semileptonic B-meson decays with form factors from lattice QCD, Phys. Rev. D **93**, 034005 (2016).

[61] R. Aaij *et al.* (LHCb Collaboration), Observation of a Resonance in $B^+ \to K^+\mu^+\mu^-$ Decays at Low Recoil, Phys. Rev. Lett. **111**, 112003 (2013).

[62] C. D. Lu and D. X. Zhang, Reexamination of long distance effects in $b \to s\ell^+\ell^-$, Phys. Lett. B **397**, 279 (1997).

[63] C. Bobeth, G. Hiller, D. van Dyk, and C. Wacker, The decay $B \to K\ell^+\ell^-$ at low Hadronic recoil and model-independent $\Delta B = 1$ constraints, J. High Energy Phys. 01 (2012) 107.

[64] C. Bobeth, G. Hiller, and G. Piranishvili, Angular distributions of $\bar{B} \to \bar{K}\ell^+\ell^-$ decays, J. High Energy Phys. 12 (2007) 040.

[65] S. Descotes-Genon, T. Hurth, J. Matias, and J. Virto, Optimizing the basis of $B \to K^*ll$ observables in the full kinematic range, J. High Energy Phys. 05 (2013) 137.

[66] S. Descotes-Genon, J. Matias, M. Ramon, and J. Virto, Implications from clean observables for the binned analysis of $B \to K^*\mu^+\mu^-$ at large recoil, J. High Energy Phys. 01 (2013) 048.

[67] D. Becirevic and E. Schneider, On transverse asymmetries in $B \to K^*l^+l^-$, Nucl. Phys. **B854**, 321 (2012).

[68] J. Matias, F. Mescia, M. Ramon, and J. Virto, Complete anatomy of $\bar{B}_d \to \bar{K}^{*0}(\to K\pi)\ell^+\ell^-$ and its angular distribution, J. High Energy Phys. 04 (2012) 104.

[69] D. Becirevic, M. Fedele, I. Nisandzic, and A. Tayduganov, Lepton flavor universality tests through angular observables of $\bar{B} \to D^{(*)}\ell\bar{\nu}$ decay modes, arXiv:1907.02257.

[70] U. Egede, T. Hurth, J. Matias, M. Ramon, and W. Reece, New physics reach of the decay mode $\bar{B} \to \bar{K}^{*0}\ell^+\ell^-$, J. High Energy Phys. 10 (2010) 056.

[71] B. Aubert *et al.* (*BABAR* Collaboration), Direct *CP*, Lepton Flavor and Isospin Asymmetries in the Decays $B \to K^{(*)}\ell^+\ell^-$, Phys. Rev. Lett. **102**, 091803 (2009).

[72] G. Hiller and F. Kruger, More model-independent analysis of $b \to s$ processes, Phys. Rev. D **69**, 074020 (2004).

[73] R. N. Faustov and V. O. Galkin, Charmless weak B_s decays in the relativistic quark model, Phys. Rev. D **87**, 094028 (2013).

[74] A. Bharucha, D. M. Straub, and R. Zwicky, $B \to V\ell^+\ell^-$ in the Standard Model from light-cone sum rules, J. High Energy Phys. 08 (2016) 098.

[75] A. Issadykov, $B_s \to K^{*0}$ decay form factors from covariant confined quark model, EPJ Web Conf. **204**, 08003 (2019).

[76] T. Kurimoto, H. N. Li, and A. I. Sanda, Leading power contributions to $B \to \pi, \rho$ transition form-factors, Phys. Rev. D **65**, 014007 (2001).

[77] H. Y. Cheng, C. K. Chua, and C. W. Hwang, Covariant light-front approach for s-wave and p-wave mesons: its application to decay constants and form factors, Phys. Rev. D **69**, 074025 (2004).

[78] W. Wang, Y. L. Shen, and C. D. Lü, Covariant light-front approach for B_c transition form factors, Phys. Rev. D **79**, 054012 (2009).

[79] Y. Y. Fan, Z. J. Xiao, R. M. Wang, and B. Z. Li, The $B \to D^{(*)}l\nu_l$ decays in the pQCD approach with the Lattice QCD input, Sci. Bull. **60**, 2009 (2015).

[80] X. Q. Hu, S. P. Jin, and Z. J. Xiao, Semileptonic decays $B_c \to (\eta_c, J/\psi)l\bar{\nu}_l$ in the "PQCD + Lattice" approach, Chin. Phys. C **44**, 023104 (2020).

[81] X. Q. Hu, S. P. Jin, and Z. J. Xiao, Semileptonic decays $B/B_s \to (D^{(*)}, D_s^{(*)})l\nu_l$ in the PQCD factorization approach with the lattice QCD input, Chin. Phys. C **44**, 053102 (2020).

[82] J. M. Flynn, T. Izubuchi, T. Kawanai, C. Lehner, A. Soni, R. S. Van de Water, and O. Witzel, $B \to \pi\ell\nu$ and $B_s \to K\ell\nu$ form factors and $|V_{ub}|$ from 2 + 1-flavor lattice QCD with domain-wall light quarks and relativistic heavy quarks, Phys. Rev. D **91**, 074510 (2015).

[83] R. R. Horgan, Z. Liu, S. Meinel, and M. Wingate, Lattice QCD calculation of form factors describing the rare decays $B \to K^*\ell^+\ell^-$ and $B_s \to \phi\ell^+\ell^-$, Phys. Rev. D **89**, 094501 (2014).

[84] P. Ball and R. Zwicky, $B_{d,s} \to \rho, \omega, K^*, \phi$ decay form-factors from light-cone sum rules revisited, Phys. Rev. D **71**, 014029 (2005).

[85] D. Melikhov and B. Stech, Weak form-factors for heavy meson decays: An update, Phys. Rev. D **62**, 014006 (2000).
[86] R. H. Li, C. D. Lu, and W. Wang, Transition form factors of B decays into p-wave axial-vector mesons in the perturbative QCD approach, Phys. Rev. D **79**, 034014 (2009).
[87] C. D. Lu, W. Wang, and Z. T. Wei, Heavy-to-light form factors on the light cone, Phys. Rev. D **76**, 014013 (2007).
[88] Y. L. Wu, M. Zhong, and Y. B. Zuo, $B_s, D_s \to \pi, K, \eta, \rho, K^*, \omega, \phi$ transition form factors and decay rates with extraction of the CKM parameters $|V_{ub}|, |V_{cs}|, |V_{cd}|$, Int. J. Mod. Phys. A **21**, 6125 (2006).
[89] F. Su, Y. L. Wu, C. Zhuang, and Y. B. Yang, Charmless $B_s \to PP, PV, VV$ decays based on the six-quark effective Hamiltonian with strong phase effects II, Eur. Phys. J. C **72**, 1914 (2012).